FINAL REPORT

(June 1st. 1994)

Fiber Optic Probes For Laser Light Scattering:
Ground Based Evaluation for Micgrogravity Flight Experimentation:

and

Integrated Coherent Imaging Fiber Optic Systems For
Laser Light Scattering and Other Applications

(NASA Grant Contract NCC3-241)
(SUNY Grant Number 431-4404A)

Award Period: 12/01/91 to 11/30/93

Principal Investigator

Harbans Singh Dhadwal
Associate Professor
State University of New York
Department of Electrical Engineering
Stony Brook, NY 11794-2350

Tel: (516) 632 8396
Fax: (516) 632 8494
email: dhadwal@sbee.sunysb.edu

CONTENTS

EXECUTIVE SUMMARY

The research work presented in this report has established a new class of a backscatter fiber optics probes for remote dynamic light scattering capability over a range of scattering angles from 94° to 175° . The fiber optic probes provide remote access to scattering systems, and can be utilized in either a noninvasive or invasive configuration. The fiber optics create an interference free data channel to inaccessible and harsh environments. Results from several studies of concentrated suspension, microemulsions and protein systems are presented.

The second part of the report describes the development of a new technology of wavefront processing within the optical fiber, that is, *integrated fiber optics.* Results have been very encouraging and the technology promises to have significant impact on the development of fiber optic sensors in a variety of fields ranging from environmental monitoring to optical recording; from biomedical sensing to photolithography.

DISSEMINATION OF RESEARCH RESULTS

PUBLICATIONS - JOURNALS

1. Romel R. Khan and Harbans S. Dhadwal, "Wavefront processing through integrated fiber optics," submitted to Optics Letters

2. Romel R. Khan and Harbans S. Dhadwal, "Generation of nondiffracting beam using selfoc lenses," submitted to Optical Fiber Technology

3. Harbans S. Dhadwal, Kwang Suh, and Romel R. Khan, "Compact backscatter fiber optic systems for submicroscopic particle sizing," submitted J. Particulate and Processing Science and Technology

4. Romel R. Khan, Harbans S. Dhadwal and Kwang I. Suh, "Design and characterization of integrated coherent fiber optic imaging probes," Applied Optics , vol 33, (1994)

5. Harbans S. Dhadwal, Romel Khan, and Kwang Suh, "Integrated fiber probes for dynamic light scattering," Applied Optics: Special Issue on Photon Correlation and Scattering, vol. 32, 3901-3904 (1993)

6. Rafat R. Ansari, Harbans S. Dhadwal, Michael Cheung, and William N. Meyer, "Microemulsion characterization by use of a noninvasive backscatter fiber optic probe," Applied Optics: Special Issue on Photon Correlation and Scattering, vol. 32, 3822-3827 (1993)

PUBLICATIONS - CONFERENCE PROCEEDINGS

7. Romel Khan and Harbans S. Dhadwal, "Integrated Imaging Fiber Optics With Multiple GRIN Lenses," Gradient Index Optical Systems Topical Meeting, June 7-8, 1994, Rochester

8. Harbans S. Dhadwal, William Wilson, Rafat Ansari, and william V. Meyer, "Dynamic light scattering studies of BSA and Lysozyme using a backscatter fiber optic system", Proceeding of the International Society of Optical Engineering: Fiber Optic Medical and Fluorescent Sensors and Applications, Los Angeles, 19-24 January 1993

9 . Harbans S. Dhadwal, Romel Khan and Kwang Suh, "Integrated coherent imaging fiber optics," Proceedings of the Tenth Topical Meeting on Gradient Index Optical Systems, Galacia, Spain; 4-6 October 1992

ABSTRACTS AND PRESENTATIONS

- Rafat R. Ansari, Harbans S. Dhadwal, H.M.Cheung, and William V. Meyer, "Microemulsion characterization using a fiber optic probe", Photon Correlation and Scattering: Theory and Applications, Eighth Topical Meeting, Boulder, Colorado, August 24-26, 1992

- Harbans S. Dhadwal, Romel Khan and Kwang Suh, "An integrated fiber optic probe for photon correlation spectroscopy", Photon Correlation and Scattering: Theory and Applications, Eighth Topical Meeting, Boulder, Colorado, August 24-26, 1992

- R.R.Ansari, Harbans S. Dhadwal, Michael Chueng, and William V. Meyer, "A fiber optic probe for the characterization of microemulsions", 9th International Symposium on Surfactants in Solution, paper #SN3.D1.2, June 10-15, 1992, Varna, Bulgaria

- R.R.Ansari, Harbans S. Dhadwal, Michael Cheung, and W.V. Meyer, "Use of a fiber optic probe for quasielastic light scattering measurements in microemulsions", paper #41 66 th Colloid and Surface Science Symposium, June 17-19 (1992), Morgantown, WV

- R.R.Ansari, Harbans S. Dhadwal, Michael Cheung, and W.V. Meyer, "Particle sizing of concentrated suspensions using a back scatter fiber optic probe," paper #92, 65 th Colloid and Surface Science Symposium, June 17-19 (1991), Norman, Oklahoma

PART I: BACKSCATTER FIBER OPTIC PROBES

Dynamic light scattering (DLS) is a noninvasive and extremely sensitive technique, which is routinely used for characterization of molecular changes in physiological, polymer, chemical, and colloidal systems. DLS characterizes the temporal fluctuations of laser light scattered by a system of particles undergoing Brownian motion or by random fluctuations in the refractive index of solutions. Temporal information is retrieved through a measurement of the time autocorrelation of the scattered light, which, in a self-beating experiment, must be collected within a single coherence solid angle. Spatial coherence requirement is a coupled function of the spectral characteristics of the optical source and the three dimensional scattering volume. Spatial coherence considerations for efficient self-beating dictates that the scattered light be collected over a small solid angle (typically, 0.1°). A conventional DLS system comprises a coherent light source, a high precision goniometer, sample cell holder, bulk optics for beam delivery and detection, a photomultiplier and digital correlator. Such systems, however, are confined to the laboratory environment, and many potentially useful areas of application are deprived of the extremely sensitive technique of DLS.

The utility and versatility of fiber optics in DLS has been established. Recent developments of backscatter fiber optic probes (BFOP) have been done at Stony Brook through support from NASA's Advanced Technology Program. Early BFOP utilized a single optical fiber for transmitting and receiving optical energy to and from the scattering region, and as such are homodyne receivers. The recent BFOP use two optical fibers for separating the transmitting and receiving paths. In this manner these BFOP are self-beating receivers with several advantages over homodyne systems; the most important being the ability to position the BFOP outside the scattering cell. Characteristics of BFOP have been studied under various conditions and for various systems. Current state-of-art for BFOP systems uses semiconductor lasers, miniature photomultipliers and notebook computers.

Reprints of the published results are attached in Appendix A; the papers under review have been listed on page 2.

PART II: INTEGRATED FIBER OPTICS

This part of the report presents a summary of the detailed study of the characterization and fabrication of integrated coherent fiber optic systems. A short length of graded index multimode fiber can have focussing properties similar to those of spherical lenses. Variation in the image distance and magnification can be obtained by controlling the length of the gradient index fiber lens (GFL) for a fixed object to lens distance.

In a typical embodiment, a monomode optical fiber is fusion spliced to a short length of a multimode gradient index optical fiber. Optical energy is confined within the core region of the latter fiber; however, the graded index profile causes a self-focussing of the optical beam, counteracting the natural divergence. The result is analogous to a series of converging lenses positioned in a confocal arrangement. The multimode optical fiber can be viewed as a series of lenses, which form a continuous guiding region. An equivalent focal length of a fiber lens will depend upon its graded index profile and length. The periodicity of the optical fiber is defined by a characteristic pitch ; a fiber lens of length equal to one pitch acts like a window, which is equivalent to a confocal arrangement of four lenses. The single most important advantage of a fiber lens is its size compatibility with monomode optical fibers, allowing the two dissimilar fibers to be fusion spliced together to form a single integrated unit, which will remain in perfect alignment for its entire life. Additionally, the integrated fiber system has a diameter which is one order of magnitude smaller than comparable systems made by using GRIN microlenses. The length of the GFL determines the imaging (non-imaging) properties of the integrated fiber optic probe. This technology has been utilized to increase the spatial resolution of BFOP described in this first part.

Reprints of the published results are attached in Appendix A; the papers under review have been listed on page 2.

APPENDIX A
REPRINTS FOR PART I

Exhibit Information (SEE PAGE 7.)

ADVANCE PROGRAM

Rochester '94 And Exhibit

Diffractive Optics: Design, Fabrication and Applications
Topical Meeting
June 6-9, 1994

International Optical Design Conference
June 6-9, 1994

Gradient Index Optical Systems
Topical Meeting
June 7-8, 1994

Optical Fabrication and Testing Workshop
June 6-9, 1994

ROCHESTER RIVERSIDE CONVENTION CENTER
Rochester, New York

Managed by the Optical Society of America

NP

INTEGRATED IMAGING FIBER OPTICS WITH MULTIPLE GRIN LENSES

Harbans S. Dhadwal and Romel R. Khan

State University of New York

Department of Electrical Engineering

Stony Brook, New York 11794-2350, USA

Tel.: 516-632-8396

FAX : 516-632-8494

ABSTRACT

An integrated imaging fiber optic probe comprising a monomode optical fiber and two short lengths of graded index multimode fibers, fusion spliced in series, has been fabricated and evaluated for remote beam delivery applications.

INTEGRATED IMAGING FIBER OPTICS WITH MULTIPLE GRIN LENSES

Harbans S. Dhadwal and Romel R. Khan
State University of New York
Department of Electrical Engineering
Stony Brook, New York 11794-2350, USA

SUMMARY

Design and fabrication of an integrated imaging fiber optic probe (IFOP) (comprising a monomode optical fiber which is fusion spliced to a short length of a graded index multimode fiber) for delivery of either a collimated beam or a focused spot to a remote location, has been reported earlier.[1] A short section of a multimode graded index fiber (GFL) with quadratic index profile has focusing properties similar to those of spherical lenses and Selfoc[2] graded index lenses manufactured by NSG[2]. Advantages of GFL over Selfoc lenses include miniaturization, narrower beam delivery for a certain distance and alignment-free lens system since the GFL is fused to the monomode fiber. Applications in areas such as photon correlation spectroscopy[3] and fiber optic connectors[4] have been evaluated. Variations in the image distance and magnification can be obtained by controlling the length of the GFL and is limited by the properties (namely the refractive index profile) of the GFL under use.

In this paper, we report the design and fabrication of an IFOP, comprising a monomode optical fiber and two GFLs fusion spliced in series (see Fig. 1). In this arrangement, greater control over image distance and magnification is obtained. Fusing more than one GFL in series would permit fiber optic in-line signal processing.

For a fiber having a quadratic refractive index profile of the form

$$n_i^2(r) = n_{0i}^2(1 - (g_{0i}r)^2) \tag{1}$$

the pitch P is given by,

$$P_i = \frac{2\pi}{g_{0i}} \tag{2}$$

where r is the radial distance from the optical axis. n_{0i} and g_0 are the on-axis refractive index and the quadratic index constant, respectively, for the ith GFL. Fractional pitch $\eta_i = L_i/P_i$ and is in the range 0 to 1.0. Equations for the image distance d_i, magnification and beam waists w_z are easily derived using the ray matrix analysis for Gaussian wave (the output of the monomode fiber can be approximated to a Gaussian profile of beam radius w_o)[5] as developed by Gomez-Reino et. al..[6,7]

$$\begin{aligned} w_z^2 &= w_o^2[(H_{22} + \dot{H}_{22}n_{o2}z)H_{21} + (H_{12} + \dot{H}_{12}n_{o2}z)\dot{H}_{21}n_{o1}/n_{o2}]^2 \\ &\quad +(\lambda/\pi w_o)^2[(H_{22} + \dot{H}_{22}n_{o2}z)H_{11}/n_{o1}(H_{12} + \dot{H}_{12}n_{o2}z)\dot{H}_{11}/n_{o2}]^2 \end{aligned} \tag{3}$$

$$d_i = -\frac{H_{22}\dot{H}_{22}K_1 + H_{12}\dot{H}_{12}K_2 + (H_{22}\dot{H}_{12} + H_{12}\dot{H}_{22})K_3}{n_{o2}[\dot{H}_{22}^2 K_1 + \dot{H}_{12}^2 K_2 + 2\dot{H}_{22}\dot{H}_{12}K_3]} \quad (4)$$

where

$$\begin{aligned} H_{1i} &= \sin(2\pi\eta_i)/g_{oi} \\ H_{2i} &= \dot{H}_{1i} = \cos(2\pi\eta_i) \\ \dot{H}_{2i} &= -g_{oi}\sin(2\pi\eta_i) \\ K_1 &= (w_o H_{21})^2 + (\frac{\lambda H_{11}}{\pi w_o n_{o1}})^2 \\ K_2 &= [(w_o \dot{H}_{21} n_{o1})^2 + (\frac{\lambda \dot{H}_{11}}{\pi w_o})^2]/n_{o2}^2 \\ K_3 &= [w_o^2 n_{o1} H_{21}\dot{H}_{21} + (\lambda/\pi w_o)^2 H_{11}\dot{H}_{11}/n_{o1}]/n_{o2} \end{aligned}$$

Magnification can be found by equating Eq. (4) and substituting $z = d_i$ in Eq. (3) and then dividing by w_o.

Table 1 shows the parameters of two multimode fibers used to fabricate an IFOP. Figures 2(a) & 2(b) show theoretical plots of the image distance d_i and magnification as a function of the fractional pitch of the second GFL which is a MSD fiber. The number associated with each curve indicates the fractional pitch of the first GFL which was a MLD fiber. We can see that by using MLD GFL with MSD GFL, the maximum d_i can be increased over using MSD GFL alone. A monomode fiber, Newport model FSV, w_0=2.3 μm, was fusion spliced to a MSD GFL 260 μm long, which was then fusion spliced to a MLD GFL 75 μm long. Laser light from a He-Ne laser, Melles Griot model GLG5261, was launched into the free end of the monomode fiber by means of a x20 microscope objective. A fiber coupled to a power meter, Newport model 835, was used to record the transverse intensity distribution at various positions, z, from the tip of the imaging probe. Figure 3 shows a comparison of the experimental (crosses) and theoretical (solid line) intensity obtained for this IFOP at (a)z = 7.62 mm and (b)z = 15.3 mm.

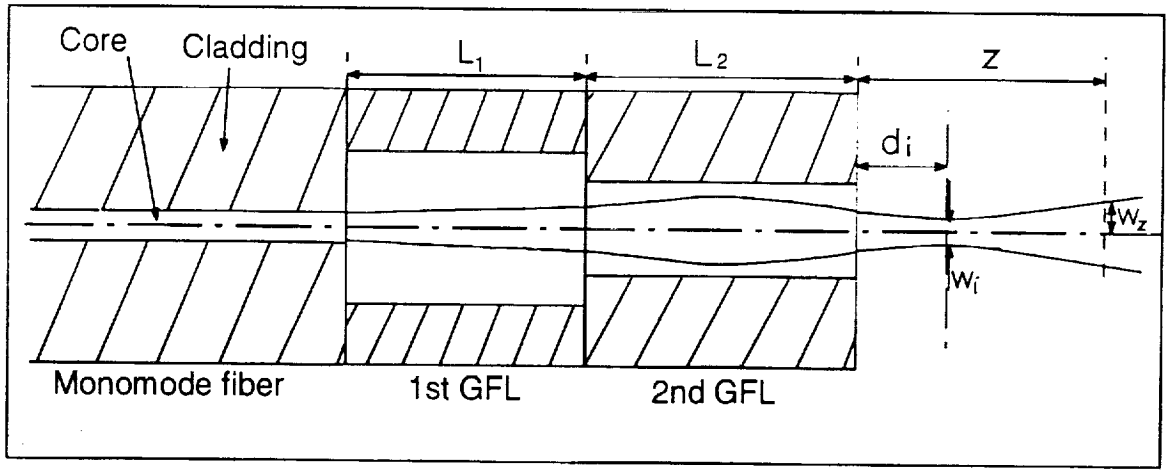

Figure 1. Schematic of an integrated imaging fiber optic probe with multiple lenses.

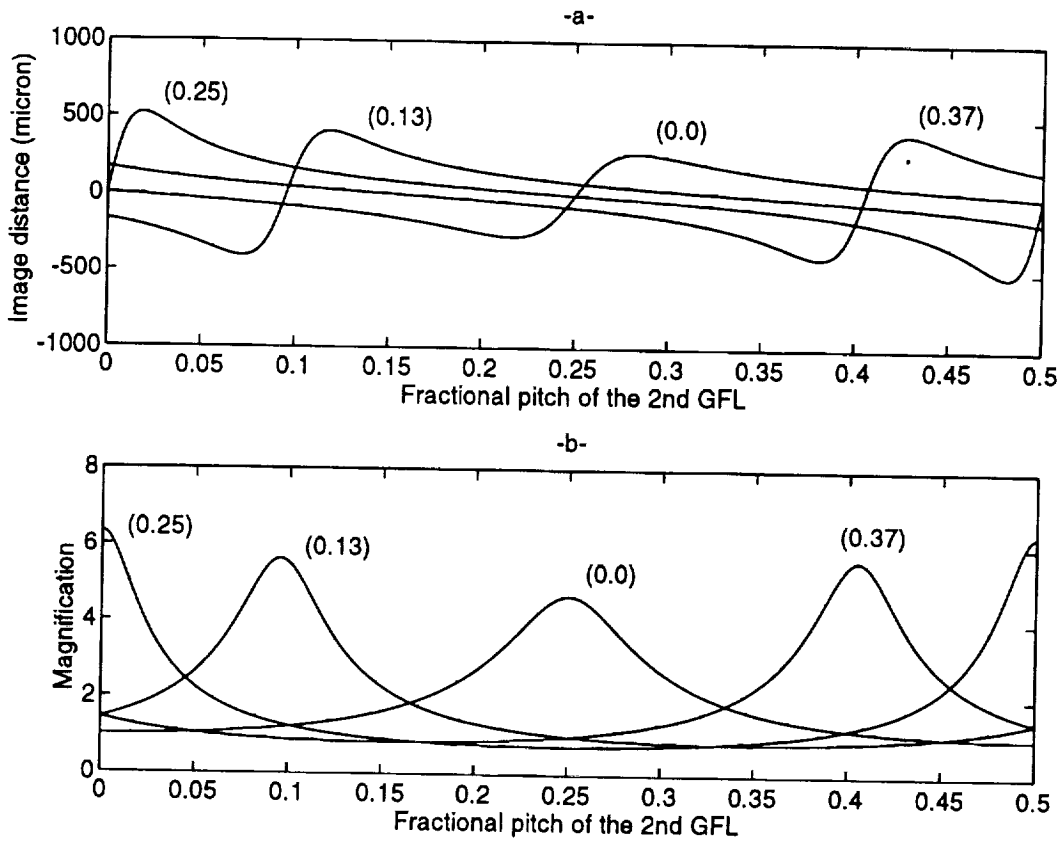

Figure 2. Theoretical plots for the imaging properties of an IFOP with MLD fiber as the 1st and MSD as the 2nd GFL. The number on each curve indicate η_1.

Fibers	n_o	$g_o(\text{mm}^{-1})$	diameter(μm)
MSD	1.4713	5.54	50
MLD	1.4815	4.05	100

Table 1: Properties of two multimode graded index fibers

In conclusion, we have described IFOP with multiple GFLs which could gain greater control in imaging properties over the single GFL case. Experimental result has been in close agreement with theoretical expectations.

REFERENCES

1. Dhadwal, Khan and Suh, 10th Topical meeting on GRIN systems, Spain (1992).
2. SELFOC is a trademark of Nippon Sheet Glass Company.
3. Dhadwal, Khan and Suh, Appl. Opt. Vol. 32, 3901-3904 (1993).
4. Emkey and Jack, J. Lightwave Tech., Vol. LT-5, 1156-1164 (1987).
5. D. Marcuse, J. Opt. Soc. Am. Vol. 68, 103-109 (1978).
6. Acosta, Flores, Gómez-Reino and Liñares, Opt. Eng., Vol. 28, 1168-1172 (1989).
7. Gómez-Reino and Liñares, Appl. Opt. Vol. 25, 3418-3424 (1986).

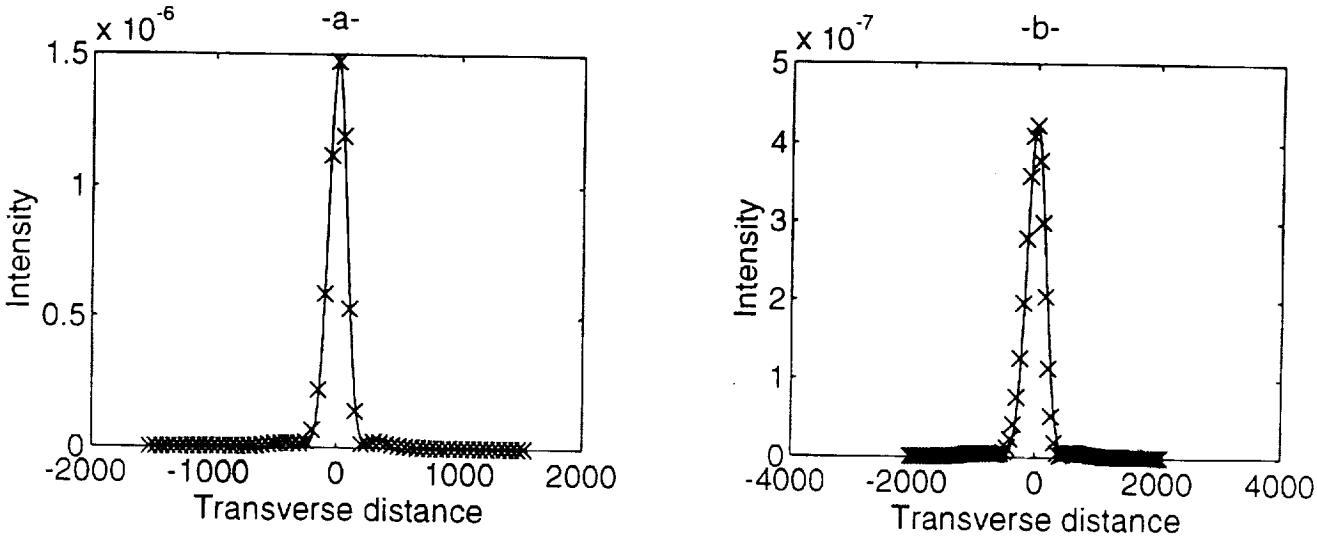

Figure 3. Experimental (crosses) and theoretical (solid line) intensity plots for an IFOP with MSD GFL of length 260 μm followed by a MLD GFL of length 75 μm at (a)$z = 7.62$ mm and (b)$z = 15.3$ mm.

Applied Optic
Under revision Accept
Vol 33 (1994)

DESIGN AND CHARACTERIZATION OF COHERENT INTEGRATED FIBER OPTIC IMAGING PROBES

Romel R. Khan, Harbans S. Dhadwal* and Kwang Suh

State University of New York

Department of Electrical Engineering

Stony Brook, New York 11794-2350, USA

NCC3-211

ABSTRACT

An integrated fiber optic probe comprising a short length of multimode fiber, fusion spliced to a monomode optical fiber, has been fabricated for imaging and non-imaging applications. The fiber probe, typically 250 μm in diameter, can deliver a focused Gaussian spot of approximately 30 μm diameter at a distance of approximately 700 μm from the tip. Two off-the-shelf graded index multimode fibers have been used in the fabrication of imaging and non-imaging probes.

*Author to whom correspondence should be addressed.

I Introduction

In this paper, we report the design and characterization of integrated fiber optic probes, comprising a monomode optical fiber, which is fusion spliced to a short length of a graded index multimode fiber, for delivery of either a collimated beam or a focused spot to a remote location. There have been several earlier works on the uses of the graded index multimode fiber lens (GFL). Dhadwal et. al.[1] used the integrated GFL probes as coherent receivers in dynamic light scattering. Emkey and Jack[2] evaluated them in connection with the development of miniaturized low-loss fiber optic connectors. Watson[3] used the GFLs to make a linear array of microlenses. Mathyssek et. al.[4] used them in laser diode to single mode fiber coupling. Liou[5] used a GFL as an external cavity to an InGaAsP buried-heterostructure laser.

We note that a multimode graded index optical fiber has focusing properties similar to those of spherical lenses and Selfoc[6] graded index lenses manufactured by NSG[6]. Advantages of GFLs include size compatibility with monomode optical fibers and an overall reduction in size by a factor of 10 over Selfoc lenses. Variation in the image distance and magnification is obtained by controlling the length L of the GFL. The object distance, in this paper, is fixed to zero since the monomode fiber is fused to the lens resulting in a rugged and compact probe which does not require alignment of the lens.

Two multimode fibers, 50/125-μm fiber (Newport model MSD) and 100/140-μm fiber (Newport model MLD), have been considered in this work. In section II GFL parameters such as beam waist and image distance are found using ray matrix analysis for a Gaussian wave. In section III experimental results are presented.

II Theoretical Background

Figure 1 shows a schematic of a generic integrated coherent fiber optic probe. The refractive index profile of the fibers considered in this paper, is of the form

$$n^2(r) = n_0^2(1 - (g_0 r)^2) \quad . \tag{1}$$

where r is the radial distance from the optical axis, n_0 is the on-axis refractive index and g_0 is the quadratic index constant. Neglecting aberration effects, the pitch P, of the fiber is given by[7]

$$P \approx \frac{2\pi}{g_0} \tag{2}$$

The optical field distribution radiating from the tip of a monomode fiber can be approximated by a Gaussian profile[8] having a beam waist (or beam radius) w_0, corresponding to the core radius of the monomode fiber, which is fusion spliced to the front surface of the multimode fiber as shown in Figure 1. In our work, we used a monomode fiber of core radius 2 μm. Following the ray matrix analysis given by Gomez-Reino et. al.,[9,10] the complex input ray position and slope for a Gaussian wave are given by $r_1 = w_0$ and $\dot{r}_1 = j\lambda/(\pi n_0 w_0)$, respectively. Here λ is the wavelength of light. The complex input is related to the complex output position r_2 and slope $\dot{r}_2$, at a distance z from the tip of the GFL (see Figure 1) by

$$\begin{pmatrix} r_2 \\ \dot{r}_2 \end{pmatrix} = \begin{pmatrix} A & B \\ C & D \end{pmatrix} \begin{pmatrix} r_1 \\ \dot{r}_1 \end{pmatrix} \tag{3}$$

where

$$\begin{pmatrix} A & B \\ C & D \end{pmatrix} = M_{43}M_{32}M_{21}$$

and

$$M_{21} = \begin{pmatrix} \cos(g_0 L) & \sin(g_0 L)/g_0 \\ -g_0 \sin(g_0 L) & \cos(g_0 L) \end{pmatrix}$$

is the transmission matrix within the GFL where L is the length of the GFL.

$$M_{32} = \begin{pmatrix} 1 & 0 \\ 0 & n_0 \end{pmatrix}$$

is the refraction matrix from from GFL to air, and

$$M_{43} = \begin{pmatrix} 1 & z \\ 0 & 1 \end{pmatrix}$$

is the transmission matrix in air.

The beam waist w_z is given by the absolute value of r_1

$$w_z^2 = w_0^2\{[\cos(2\pi\eta) - n_0 z g_0 \sin(2\pi\eta)]^2 + a^2[\frac{\sin(2\pi\eta)}{g_0} + n_0 z \cos(2\pi\eta)]^2\} \tag{4}$$

where the fractional pitch $\eta = L/P$ and is in the range 0 to 1.0, and $a = \lambda/(\pi n_0 w_0^2)$.

Minimizing w_z with respect to z, gives image distance d_i and image magnification m_g[11]

$$d_i = \frac{\sin(4\pi\eta)[g_0^2 - a^2]}{2n_0 g_0[g_0^2 \sin^2(2\pi\eta) + a^2 \cos^2(2\pi\eta)]} \tag{5}$$

$$m_g = \frac{w_i}{w_0} = \frac{1}{[(\frac{g_0 \sin(2\pi\eta)}{a})^2 + \cos^2(2\pi\eta)]^{1/2}} \tag{6}$$

The divergence angle of the output Gaussian beam from the image point is inversely proportional to image beam waist w_i and is given by

$$\Delta\theta = \frac{\lambda}{\pi w_i} = \frac{\lambda}{\pi w_0 m_g}. \tag{7}$$

Figures 2 and 3 show plots of the image distance d_i and magnification m_g as a function of η for MLD and MSD fibers, respectively, whose characteristic parameters are shown in table I. All results are at a wavelength of 0.633 μm. From the figures we can see that for $\eta = 0.25$ the image is formed on the lens surface and the magnification is largest; therefore, the divergence is the least. Such a GFL is best for producing a collimated output. In general, figures 2 and 3 can be used for fabricating an integrated fiber probe with desired imaging condition based upon the image distance, magnification and divergence requirements.

Figure 4 shows a plot of w_z as a function of z for $0.25P$ MSD GFL (dashed line) and $0.25P$ MLD GFL (solid line). We note that divergence of the MLD GFL is lower than that of MSD GFL. For $z < 4$ mm, beam waist of less than 50 μm can be obtained.

Maximum image distance d_{im} at $\eta = \eta_m$, can be found analytically from Eq. (5) by maximizing d_i with respect to η,

$$\eta_m = \frac{1}{2\pi}\tan^{-1}(-\frac{a}{g_0}) \tag{8}$$

$$d_{im} = \frac{a^2 - g_0^2}{2n_0 a g_0^2} \tag{9}$$

For MSD GFL $\eta_m = 0.275$ and $d_{im} = 384$ μm while for MLD GFL $\eta_m = 0.269$ and $d_{im} = 697$ μm. Theoretical prediction for the intensity distribution at distance z from the tip of the GFL, is given by[11]

$$I_z = I_0 \exp(-\frac{2r^2}{w_z^2}) \tag{10}$$

where w_z is given by Eq. (4).

As mentioned earlier, the theory presented above is derived using ray matrices. For GFLs, which have a diameter comparable with the wavelength of light, diffraction effects

must be taken into account. Using diffraction analysis given by Liñares et. al.,[12,13] the intensity distribution I_d, for $L > 0.25P$ on the tip of the GFL (z=0) is given by

$$I_d = \begin{cases} |\psi_{nd} + D_1|^2, & |v| < |u| \\ |D_2|^2, & |v| > |u| \end{cases} \tag{11}$$

where

$$v = \frac{kn_0 r_0 \rho}{R_1}$$

$$u = (\frac{kn_0 R_2}{R_1} + j\frac{2}{w_1^2})r_0^2$$

where r_0 is the core radius, ρ is the radial coordinate at the tip of the GFL,

$$w_1 = \begin{cases} w_0, & 0 < \eta \leq 0.25 \\ 2/(kn_0 w_0 g_0), & 0.25 < \eta \leq 0.5 \end{cases}$$

$$R_2 = \begin{cases} \cos(2\pi\eta), & 0 < \eta \leq 0.25 \\ \cos(2\pi(\eta - 0.25)), & 0.25 < \eta \leq 0.5 \end{cases}$$

$$R_1 = \begin{cases} \sin(2\pi\eta)/g_0, & 0 < \eta \leq 0.25 \\ \sin(2\pi(\eta - 0.25))/g_0, & 0.25 < \eta \leq 0.5 \end{cases}$$

ψ_{nd} is the diffraction-free electric field distribution

$$\psi_{nd} = \frac{w_0}{w_2}\exp(-\frac{\rho^2}{w_2^2} + j(C_1 + \phi + \frac{kn_0\rho^2}{2C_2})) \tag{12}$$

where

$$C_1 = \begin{cases} -\pi/2, & 0 < \eta \leq 0.25 \\ -\pi, & 0.25 < \eta \leq 0.5 \end{cases}$$

$$\phi = \tan^{-1}(\frac{kn_0 R_2 w_1^2}{2R_1})$$

$$w_2^2 = \frac{4R_1^2 + k^2 n_0^2 R_2^2 w_1^4}{k^2 n_0^2 w_1^2}$$

$$\frac{1}{2C_2} = \frac{R_2}{2R_1} - \frac{k^2 n_0^2 w_1^4 R_2}{2R_1(4R_1^2 + k^2 n_0^2 R_2^2 w_1^4)}$$

D_1 and D_2 are the diffraction terms

$$D_1 = \frac{w_0}{w_2} \exp(j(\phi + \frac{k n_0 R_2 \rho^2}{2R_1} + \frac{u}{2}))L_1 \quad . \tag{13}$$

$$D_2 = \frac{w_0}{w_2} \exp(j(\phi + \frac{k n_0 R_2 \rho^2}{2R_1} + \frac{u}{2}))L_2 \tag{14}$$

where

$$L_1 = \begin{cases} V_1(u,v) + jV_0(u,v), & 0 < \eta \leq 0.25 \\ V_0(u,v) - jV_1(u,v), & 0.25 < \eta \leq 0.5 \end{cases}$$

$$L_2 = \begin{cases} -U_1(u,v) + jU_2(u,v), & 0 < \eta \leq 0.25 \\ U_2(u,v) + jU_1(u,v), & 0.25 < \eta \leq 0.5 \end{cases}$$

and $U_n(u,v)$ and $V_n(u,v)$ are the Lommel functions described in Born and Wolf[14]

$$U_n(u,v) = \sum_{s=0}^{\infty} (-1)^s (\frac{u}{v})^{n+2s} J_{n+2s}(v)$$

$$V_n(u,v) = \sum_{s=0}^{\infty} (-1)^s (\frac{v}{u})^{n+2s} J_{n+2s}(v)$$

The input field distribution I_i is given by

$$I_i = \exp(-\frac{\rho_0^2}{w_0^2})$$

where ρ_0^2 is the radial coordinate at the input plane. Note that ω_0 defined in Gomez et. al.[12] is the input intensity beam waist, while w_0 in this paper is the input field beam waist which is approximated to the core radius of the fiber.

Let the range of measurable signal be taken within $\rho \leq w_2$; that is, the measurable diffraction-free intensity distribution I_{nd} (or $|\psi_{nd}|^2$) be within 1 to exp(−2). Now we define the rms relative error due to diffraction as

$$\epsilon = \sqrt{\frac{\int_0^{w_2}(I_d - I_{nd})^2 d\rho}{\int_0^{w_2} I_{nd}^2 d\rho}} \tag{15}$$

Using Eqs. (11)-(13), Eq. (15) can be written as

$$\epsilon = \sqrt{\frac{\int_0^{w_2}(|D_1|^2 + 2|\psi_{nd}||D_1|\cos(\phi_1 - \phi_2))^2 d\rho}{\int_0^{w_2} I_{nd}^2 d\rho}} \tag{16}$$

where

$$\phi_1 = C_1 - \frac{k^3 n_0^3 w_1^4 R_2 \rho^2}{2R_1(4R_1^2 + k^2 n_0^2 R_2^2 w_1^4)}$$

and

$$\phi_2 = \frac{k n_0 R_2 r_0^2}{2R_1} + \tan^{-1}\left(\frac{Im(L1)}{Re(L1)}\right)$$

where $Im(.)$ is the imaginary value of the argument and $Re(.)$ is the real value of the argument.

Using Eq. (16), we found that for MSD GFL, $\epsilon < 3\%$ and for MLD GFL, $\epsilon < 0.02\%$ for $0 < \eta \leq 0.5$ at $\lambda = 0.633$ μm; therefore, for these two GFLs diffraction effects are negligible.

III. Experimental procedure and results

Details of the fabrication process for an integrated fiber probe is described in Dhadwal et. al.[1] and will not be repeated here. Figure 5 shows a schematic of the system for characterizing a GFL. A He-Ne laser (Melles Griot model GLD5261) was launched into the free end of the monomode fiber by means of a 20x microscope objective. A fiber coupled to a power meter (Newport model 835) was used to record the transverse intensity distribution at various positions z.

Figures 6 to 8 shows the theoretical (solid line) and experimental (circles) intensity vs. transverse distance relationship for MLD $0.225P$, MLD $0.255P$, and MSD $0.23P$ GFLs, respectively. The crosses on these figures show the experimental readings with an unlensed monomode fiber, confirming that the lensed fibers are producing narrower beams. The dashed lines in these figures are the expected output from a $0.25P$ GFL. The dashed and solid lines of Figure 7 are almost superimposed since the length of MLD $0.255P$ GFL is very close to $0.25P$. All intensity distributions shown, except for Figure 8, are taken at $z = 33$ mm. Distributions in Figure 8a and 8b were taken at $z = 7.6$ mm and $z = 25.4$ mm, respectively. From Figure 8, it is clear that the spot size of the unlensed fiber is growing at a greater rate implying larger divergence than lensed fibers. Another point to note is that the match between theory and experiment remains consistent for different distances.

The figures show good agreement between theory and experiment. MLD GFLs seem to show greater aberration and/or excitation of higher order modes than MSD GFLs.

IV. Summary

We have described the design of integrated fiber optic imaging probes. For the GFLs considered in this paper, maximum image distance of about 700 μm can be achieved with a magnification of about 8. For detection distance less than 4 mm, beam waist of less than 50 μm can be obtained. Experimental results have been in close agreement with theoretical expectations. Such probes can be customized for a variety of diverse applications. However, by fabricating multimode fibers with desired index profiles optimization in the parameters could be achieved; for example, greater image distance could be obtained by lowering the value of g_0.

Acknowledgement

Authors are very thankful to Dr. William Emkey of AT&T Bell Laboratories at Breinigsville for allowing access to the fusion splicer, and to Curtis Jack for his assistance and patience in using the splicer. Authors wish to acknowledge the continuous support from NASA under contract number NCC3-241.

REFERENCES

1. H. S. Dhadwal, R. R. Khan and K. Suh, "An Integrated Fiber Optic Probe For Dynamic Light Scattering," Appl. Opt. special issue on Photon Correlation Spectroscopy, (1993).

2.W. L. Emkey and C. A. Jack, "Analysis and evaluation of graded index fiber lenses," J. Lightwave. Tech. **LT-5**, 1156-1164 (1987).

3. H. Watson, "A linear array of twelve graded-index lenses butted coaxially against single mode fibers using silicon V-groove technology," in Active and Passive Fiber Workshop, 1991 (Optical Society of America, Washington, D.C., 1991), pp 149.

4. K. Mathyssek, R. Keil and E. Clement, "New coupling arrangement between laser diode and single mode fiber with high coupling efficiency and particularly low feedback effect," in *Optical Communication, ECOC '84*, H. Haupt, Editor, (North-Holland, New York, 1984), pp 186-187.

5. K. Y. Liou, "Single-longitudinal-mode operation of injection laser coupled to a grinrod external cavity," Electr. Lett. **19**, 750-751 (1983).

6. SELFOC is a trademark of Nippon Sheet Glass Company, Osaka, Japan.

7. Takanori Okoshi,*Optical Fibers* (Academic Press, New York, 1982), Chap 2 & 3.

8. D. Marcuse, "Gaussian approximation of the fundamental modes of graded-index fibers," J. Opt. Soc. of Amer. **68**, 103-109 (1978).

9. Acosta, Flores, Gómez-Reino, and Liñares, "Gradient index lens law for gaussian illumination: image and focal shifts," Opt. Eng. **28**, 1168-1172 (1989).

10. C. Gómez-Reino and J. Liñares, "Paraxial fourier transforming and imaging properties of a GRIN lens with revolution symmetry: GRIN lens law," Appl. Opt. **25**, 3418-3421

(1986).

11. H. S. Dhadwal, R. R. Khan and K. Suh, "Integrated Coherent Imaging Fiber Optics," in Tenth Topical Meeting on Gradient-Index Optical Systems, Technical Digest (Santiago de Compostela, Galicia, Spain, 1992), pp 23-26.

12. J. Liñares and C. Gómez-Reino, "Diffraction-limited coupling efficiency between SMF connected by GRIN fiber lenses," J. Mod. Opt. **38**, 597-604 (1991).

13. J. Liñares and C. Gómez-Reino, "Pupil effect in a GRIN lens with Gaussian illumination," J. Mod. Opt. **38**, 481-494 (1991).

14. M. Born and E. wolf, *Principles of Optics* (Pergamon Press, New York, 1980).

Figure Captions

Figure 1. Schematic of an integrated fiber optic probe.

Figure 2. Theoretical plots for the imaging properties of MLD GFL at $\lambda = 0.633$ μm. (a) Image distance d_i vs fractional pitch η, Eq. (5), and (b) Image magnification m vs fractional pitch η, Eq. (6).

Figure 3. Theoretical plots for the imaging properties of MSD GFL at $\lambda = 0.633$ μm. (a) Image distance d_i vs fractional pitch η, Eq. (5), and (b) Image magnification m vs fractional pitch η, Eq. (6).

Figure 4. Theoretical plots of beam waist w_z vs axial distance z for a $0.25P$ lens using Eq. (4) at $\lambda = 0.633$ μm. Solid line represents MLD GFL and dashed line represents MSD GFL.

Figure 5. Schematic of the system for characterizing a GFL.

Figure 6. Characterization of the intensity distribution for MLD GFL with $0.225P$ length. o – measured data points at $z = 33$ mm, Solid line – expected distribution using Eq. (10), dashed line – expected distribution for a $0.25P$ lens, x – measured data from an unlensed monomode fiber at $z = 33$ mm.

Figure 7. Characterization of the intensity distribution for MLD GFL with $0.255P$ length. o – measured data points at $z = 33$ mm, Solid line – expected distribution using Eq. (10), dashed line – expected distribution for a $0.25P$ lens, x – measured data from an unlensed monomode fiber at $z = 33$ mm.

Figure 8. Characterization of the intensity distribution for MSD GFL with $0.23P$ length. (a) $z = 7.6$ mm and (b) $z = 25.4$ mm. o – measured data points, Solid line – expected distribution using Eq. (10), dashed line – expected distribution for a $0.25P$ lens, x – measured

data from an unlensed monomode fiber.

Table I. Some characteristic parameters of MSD fiber and MLD fiber. All data are at wavelength 0.633 μm.

Fiber type	n_0	g_0 (mm^{-1})	Diameter.d (mm)	On axis N.A
MSD	1.4655	5.46	0.050	0.2
MLD	1.4815	4.05	0.1	0.3

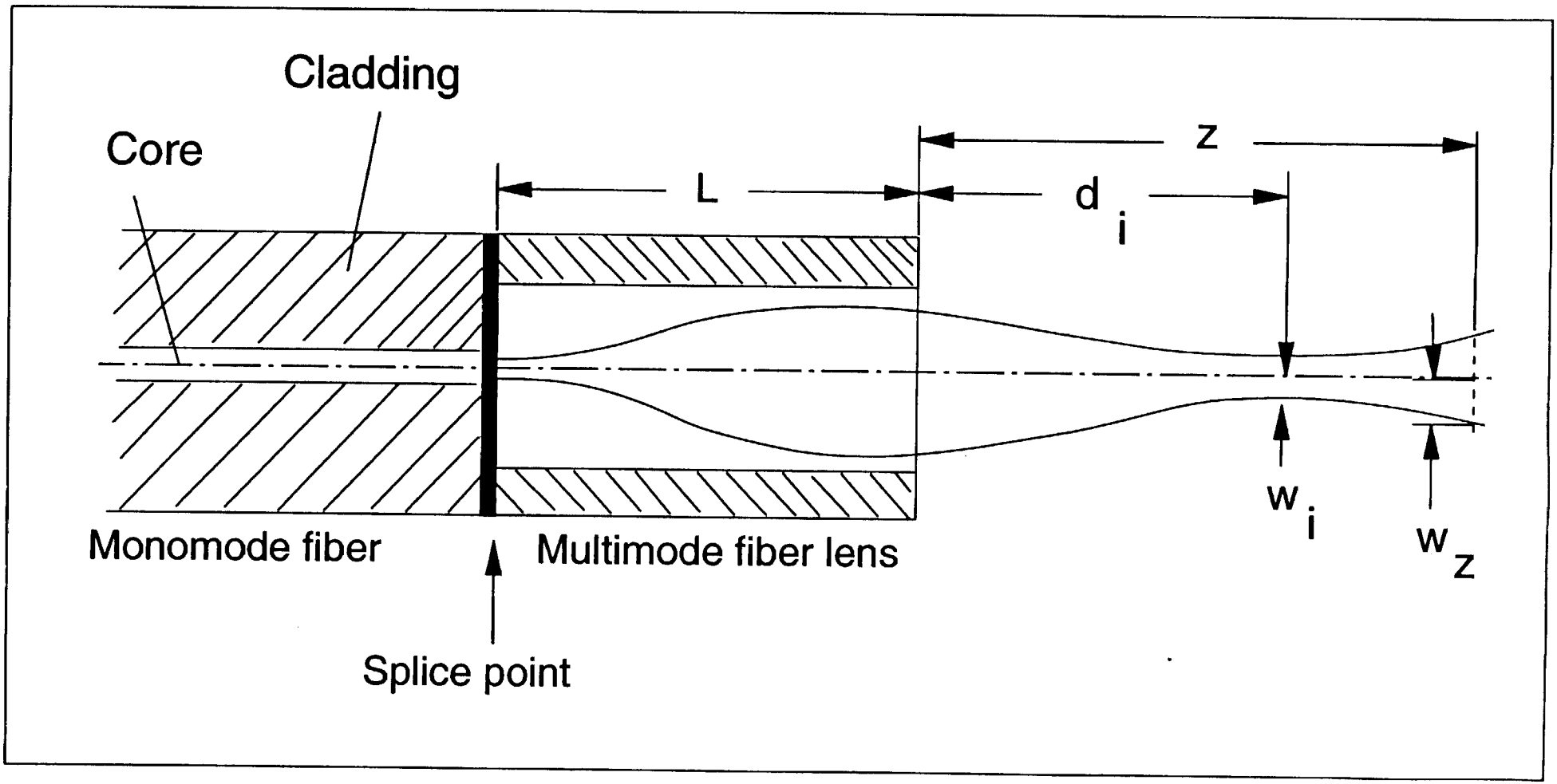
Cladding
Core
L
z
d
i
w
i
w
z
Monomode fiber
Multimode fiber lens
Splice point

Fig.1

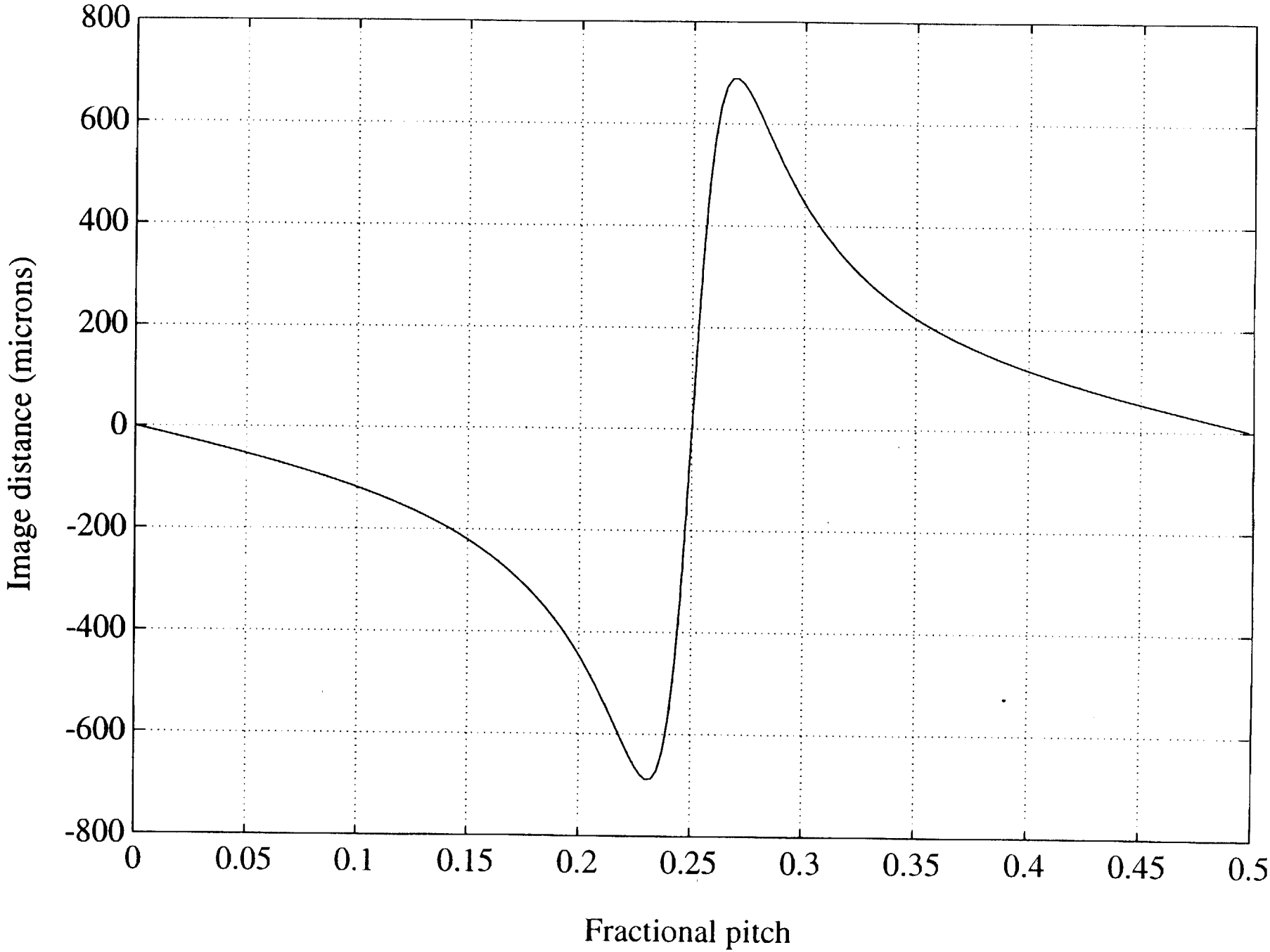
800
600
400
200
0
-200
-400
-600
-800
Image distance (microns)
0
0.05
0.1
0.15
0.2
0.25
0.3
0.35
0.4
0.45
0.5
Fractional pitch

Fig 2a

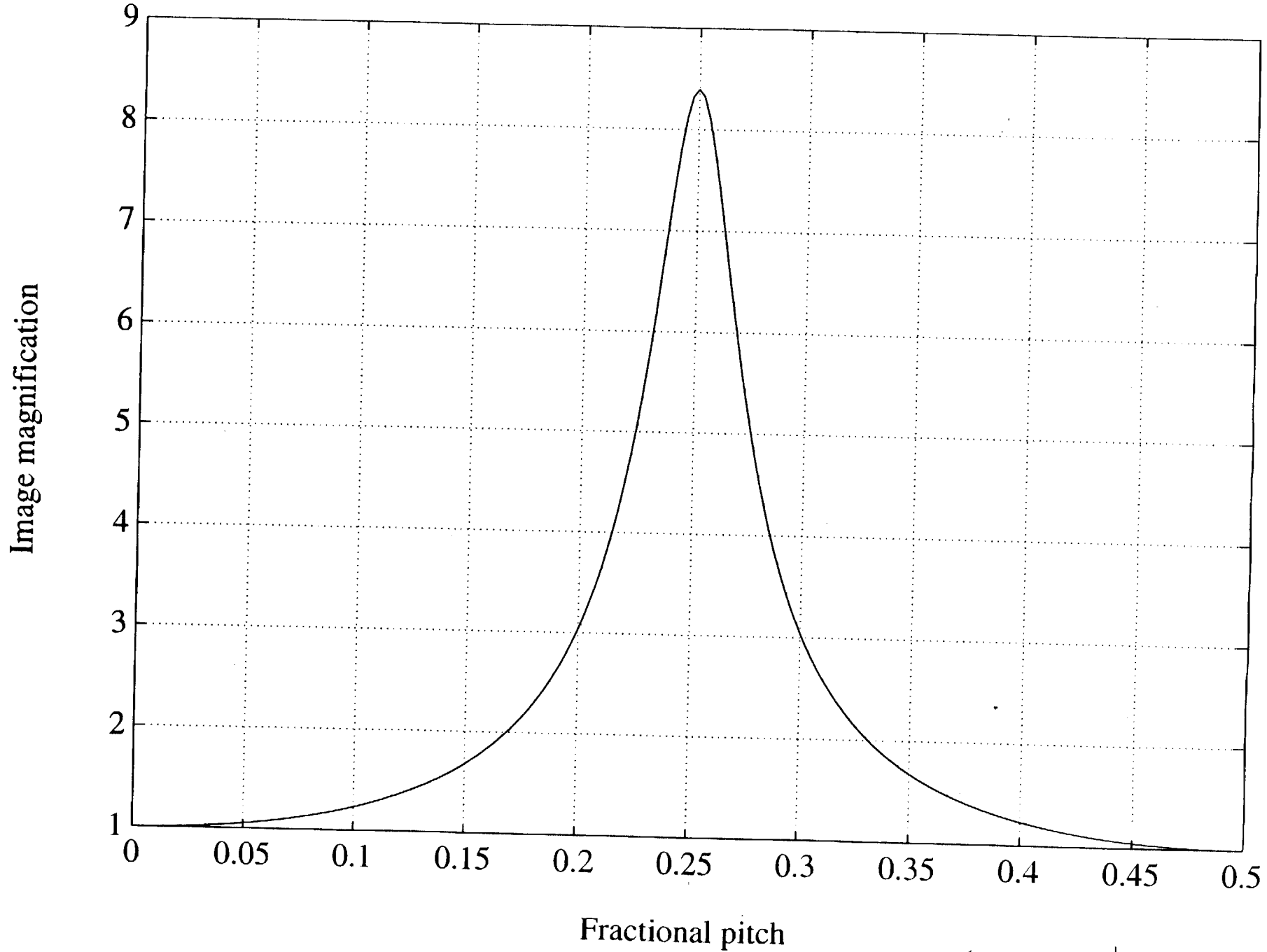
Image magnification
9
8
7
6
5
4
3
2
1
0
0.05
0.1
0.15
0.2
0.25
0.3
0.35
0.4
0.45
0.5
Fractional pitch

Fig 2 L)

Fig 2b

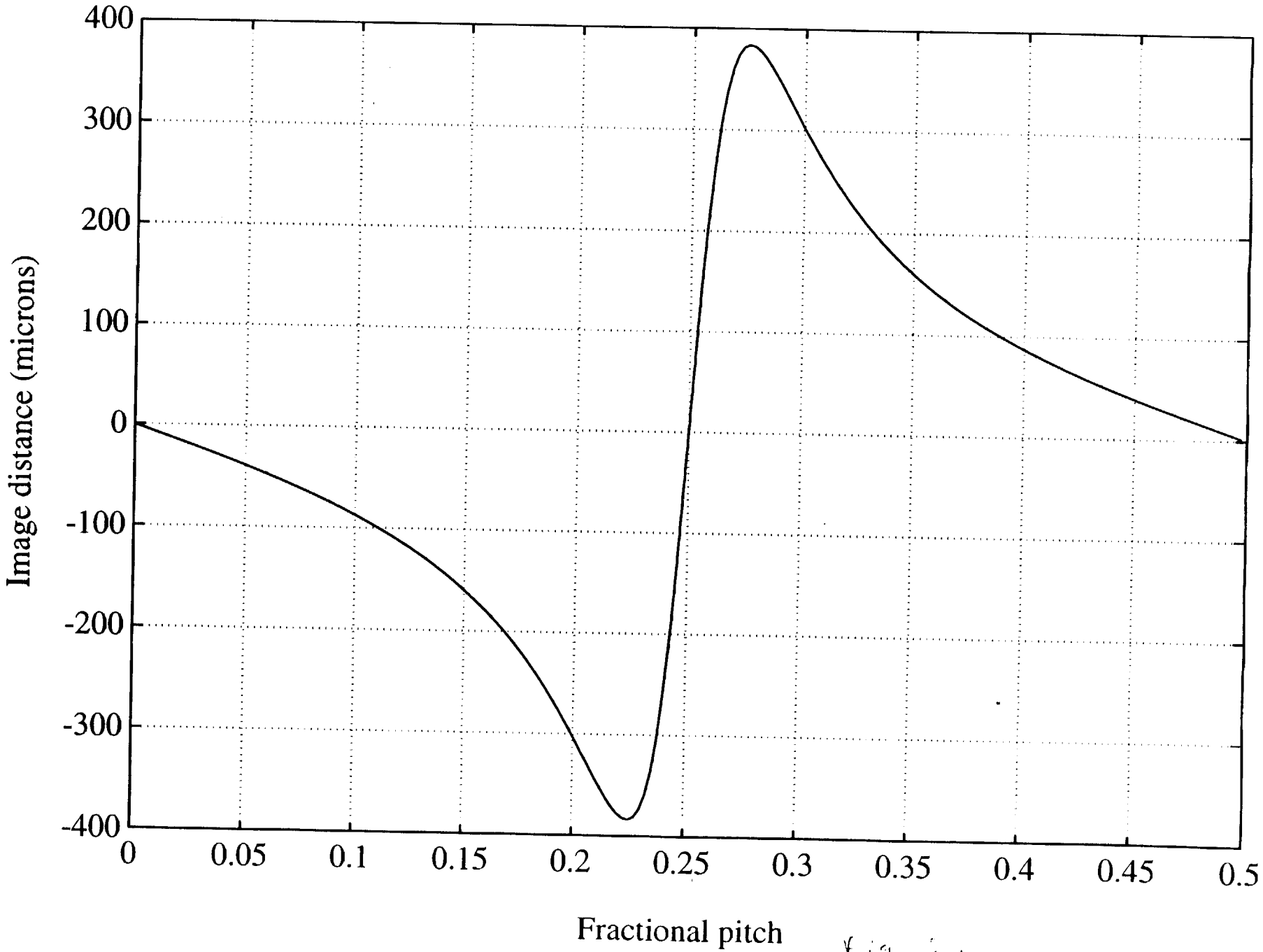
400
300
200
100
0
-100
-200
-300
-400
Image distance (microns)
0
0.05
0.1
0.15
0.2
0.25
0.3
0.35
0.4
0.45
0.5
Fractional pitch

Fig 3a

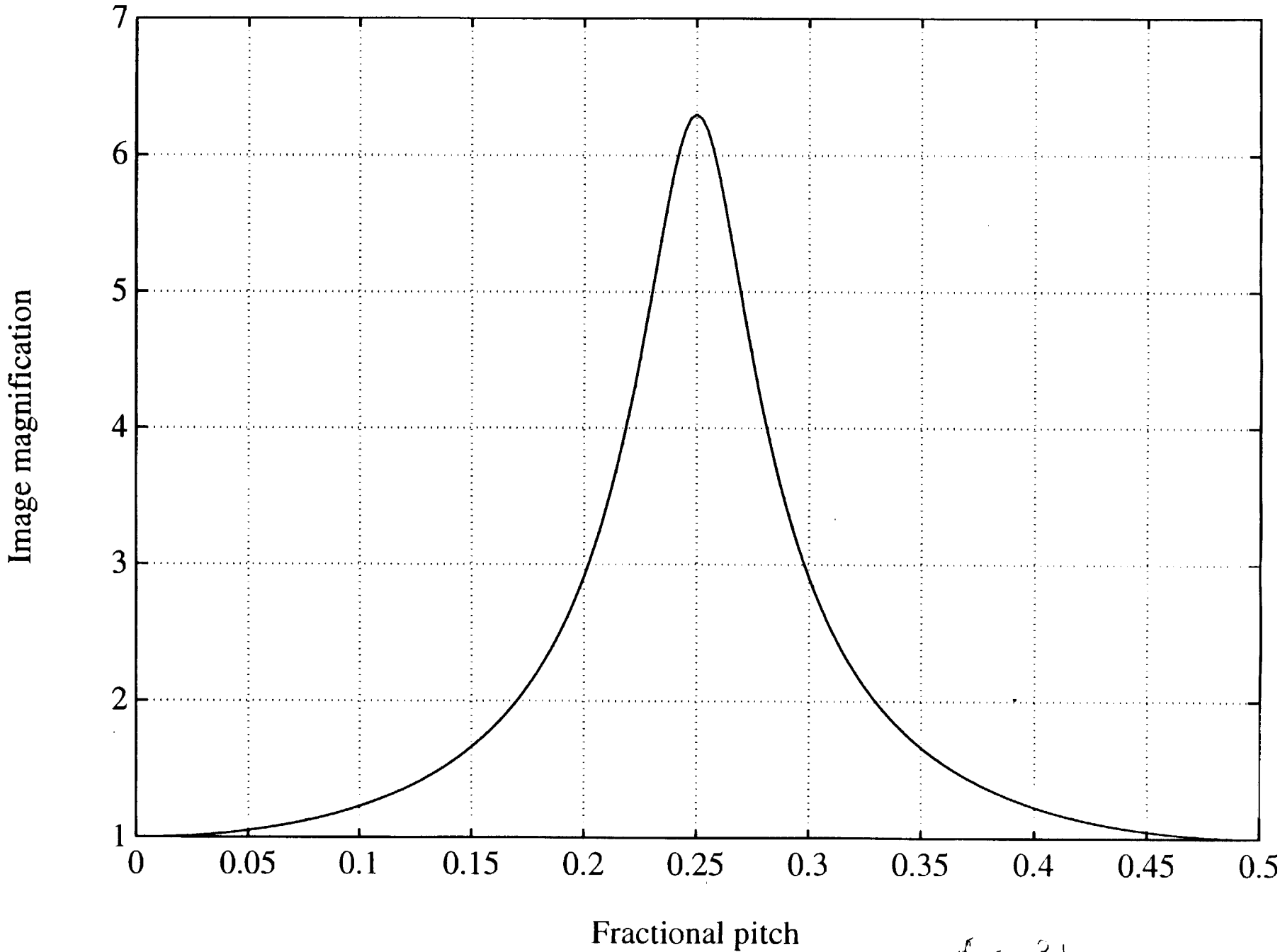
Image magnification
7
6
5
4
3
2
1
0
0.05
0.1
0.15
0.2
0.25
0.3
0.35
0.4
0.45
0.5
Fractional pitch

Fig 3b

Fig 3b

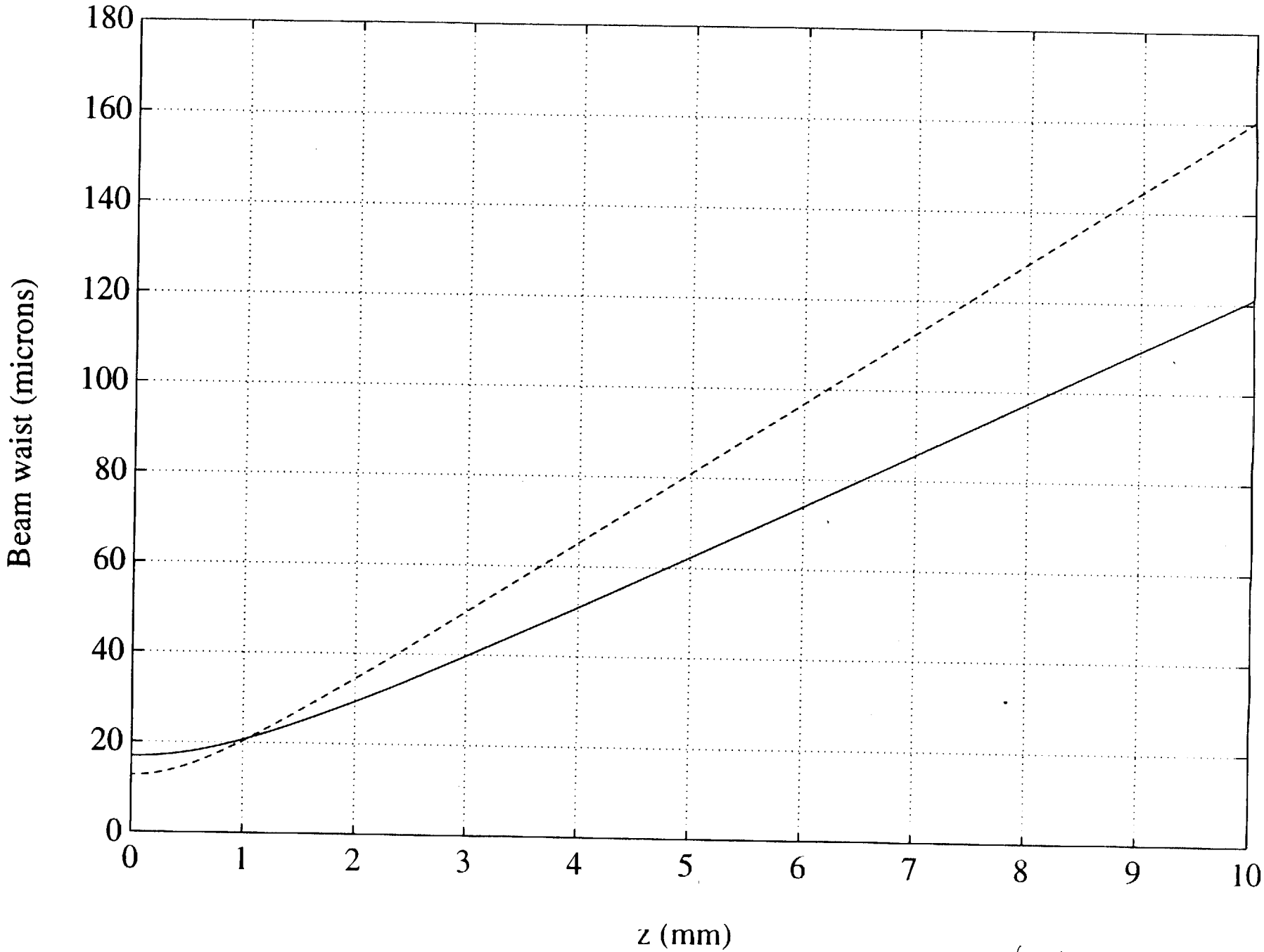
Beam waist (microns)
z (mm)
0
20
40
60
80
100
120
140
160
180
0
1
2
3
4
5
6
7
8
9
10

fig 4

Fig 4

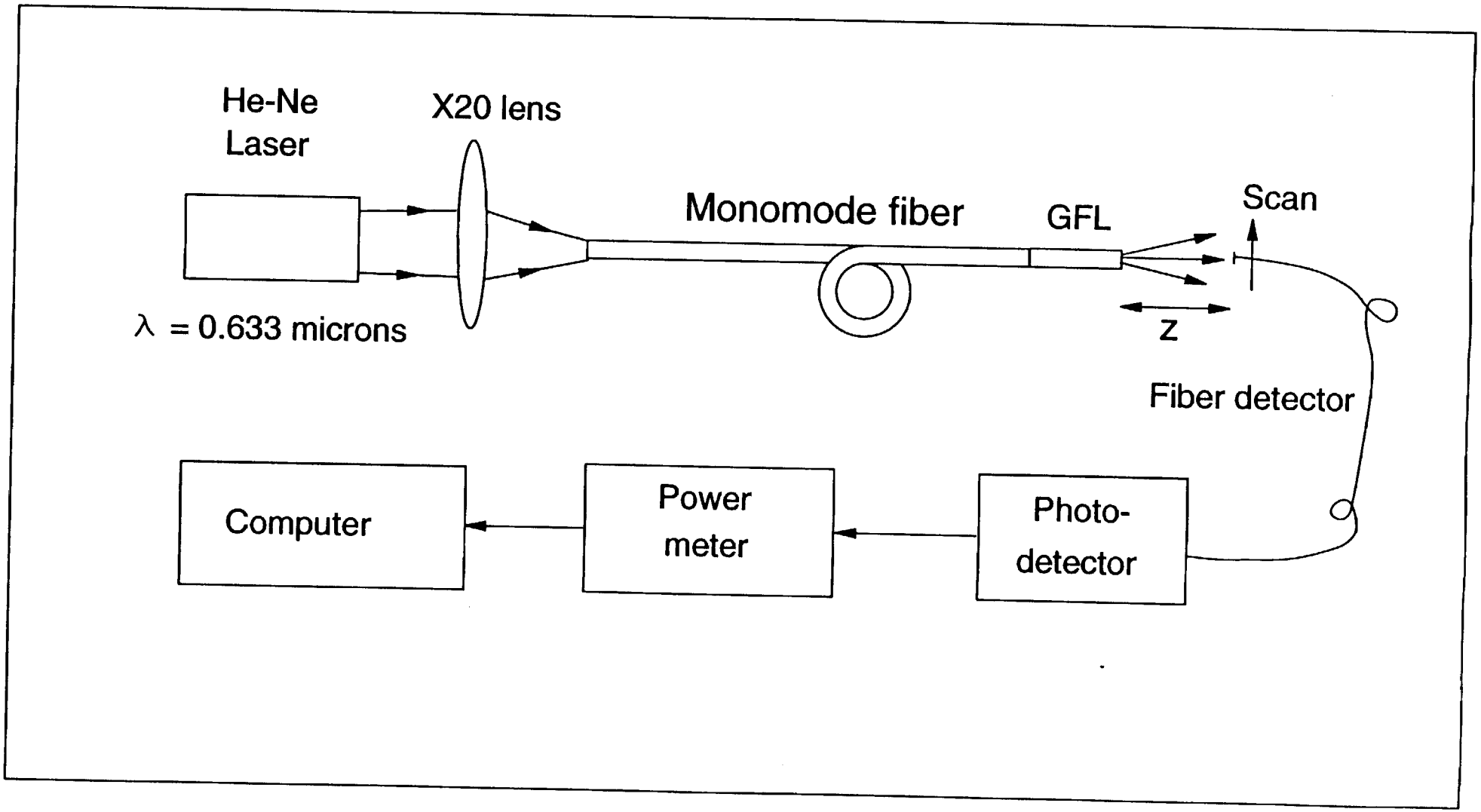
He-Ne
Laser
X20 lens
Monomode fiber
GFL
Scan
λ = 0.633 microns
z
Fiber detector
Computer
Power
meter
Photo-
detector

Fig 5

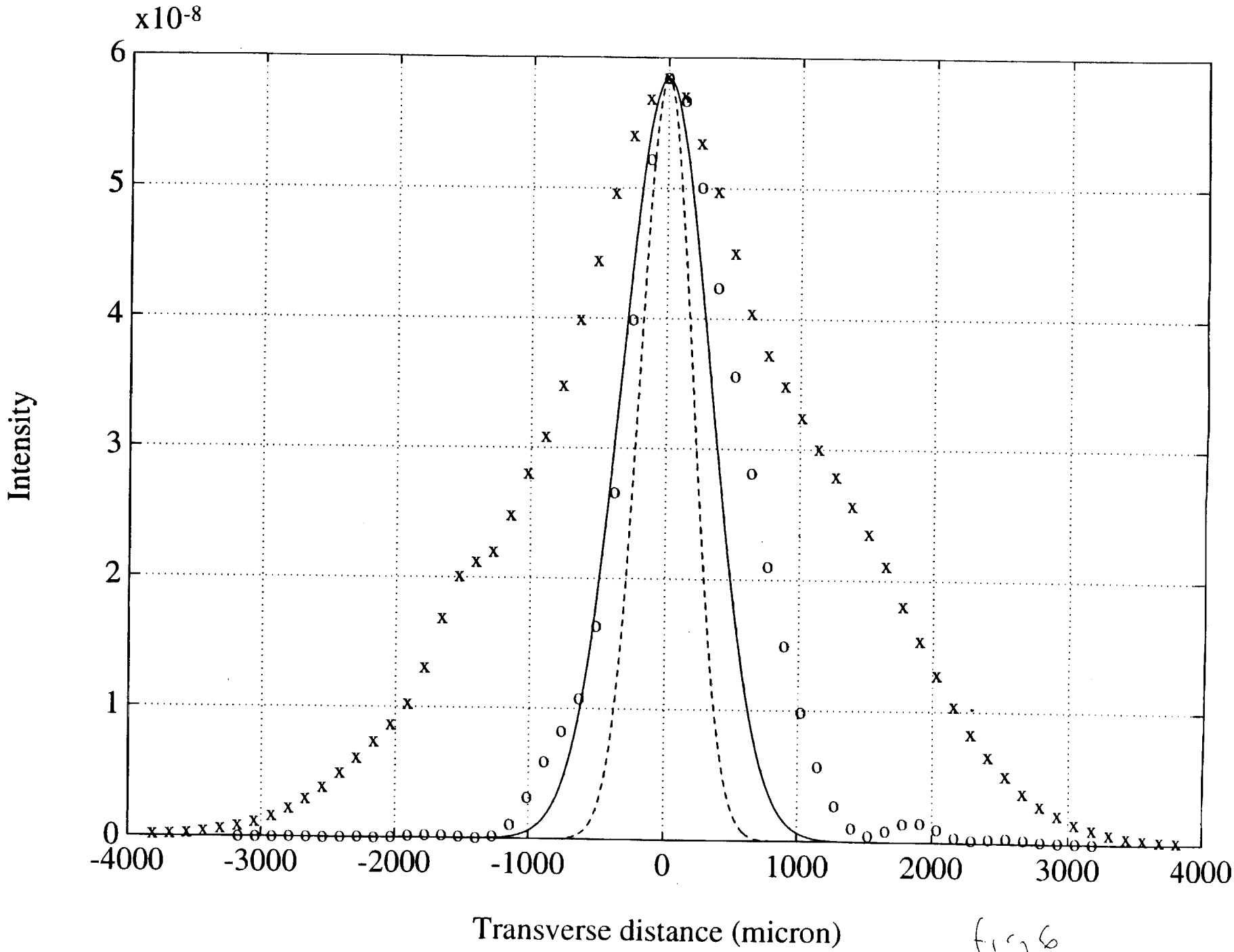
x10-8
6
5
4
3
2
1
0
Intensity
-4000
-3000
-2000
-1000
0
1000
2000
3000
4000
Transverse distance (micron)

fig 6

Fig 6

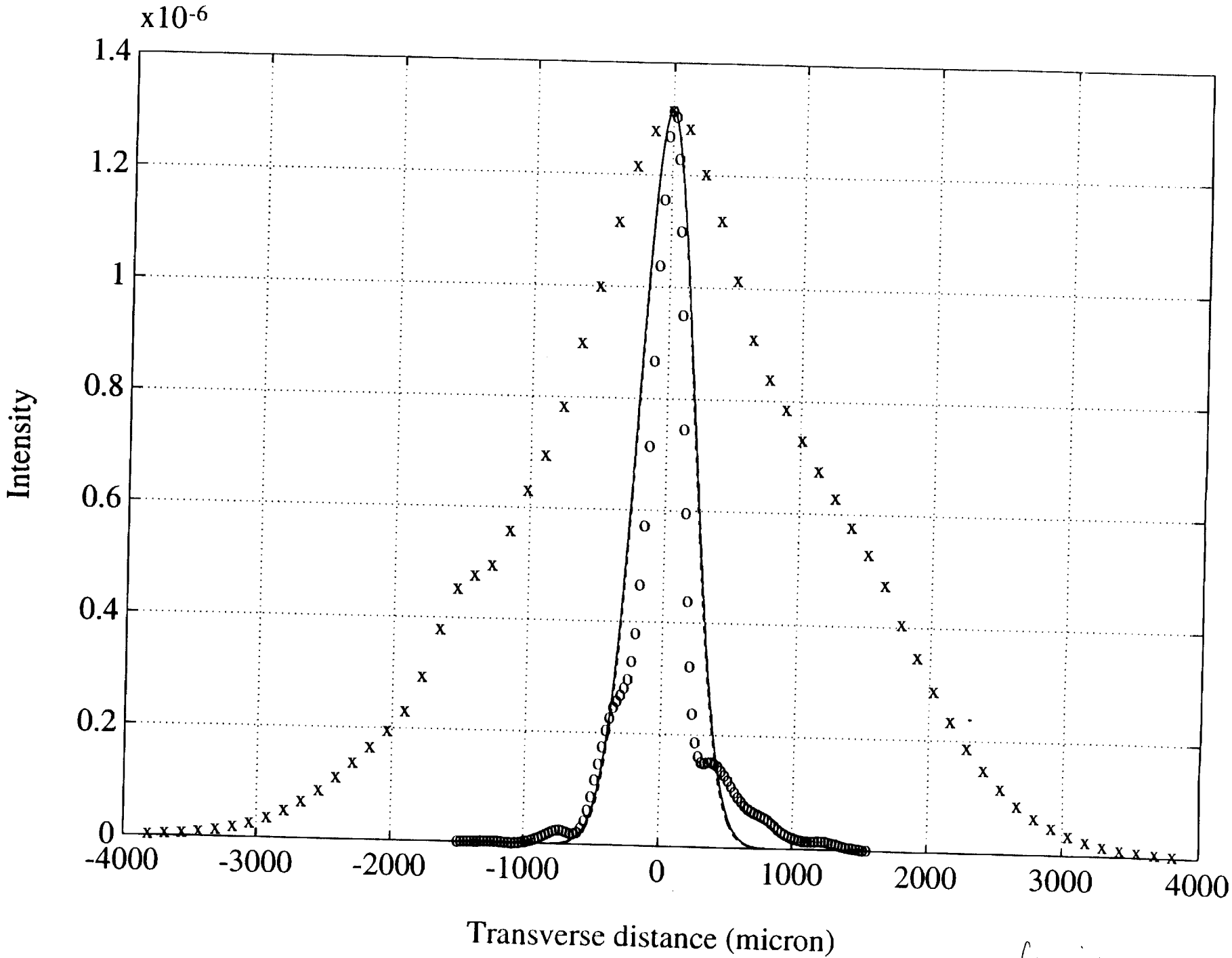
x10-6
1.4
1.2
1
0.8
0.6
0.4
0.2
0
Intensity
-4000
-3000
-2000
-1000
0
1000
2000
3000
4000
Transverse distance (micron)

fig 1

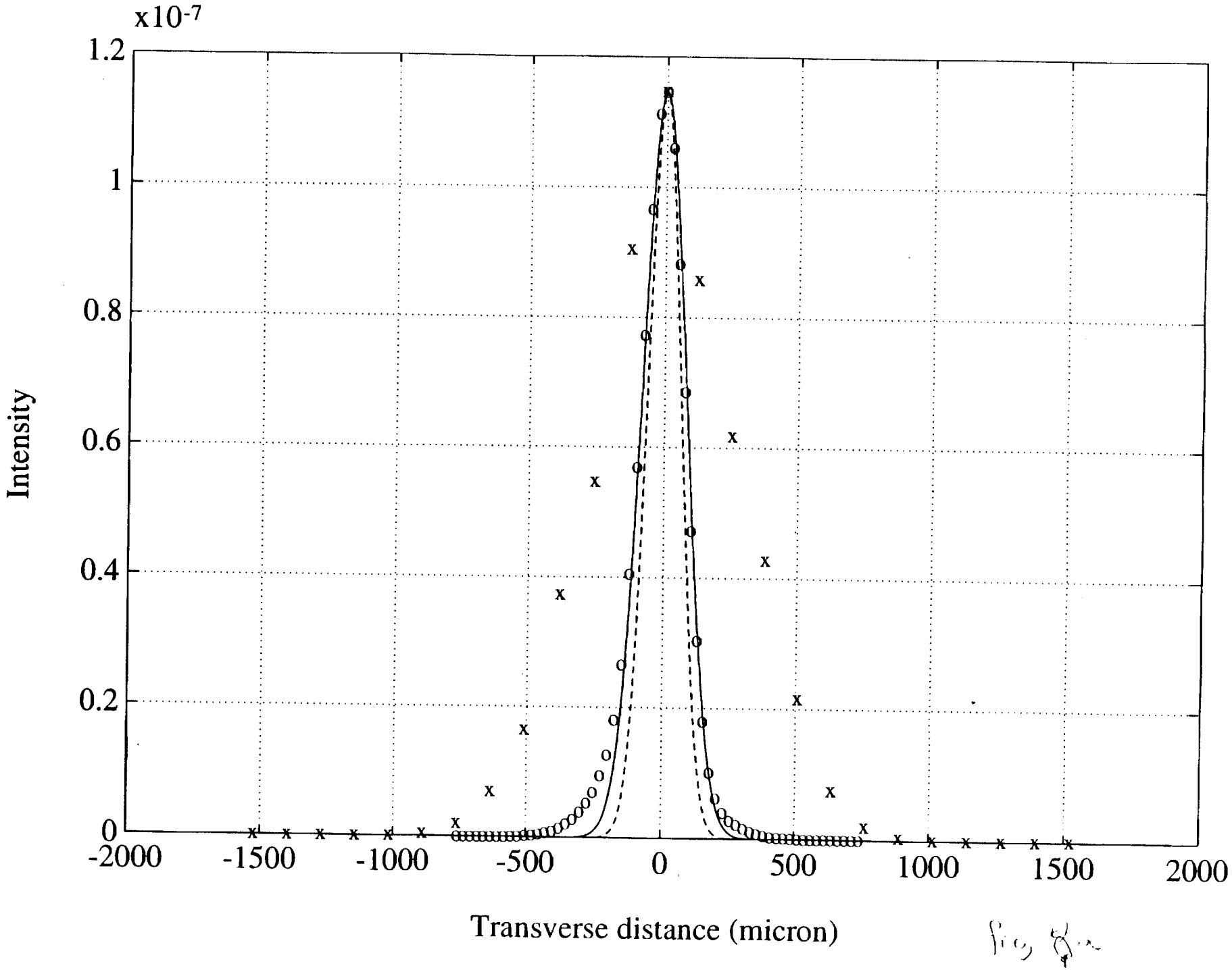
x10-7
1.2
1
0.8
0.6
0.4
0.2
0
Intensity
-2000
-1500
-1000
-500
0
500
1000
1500
2000
Transverse distance (micron)

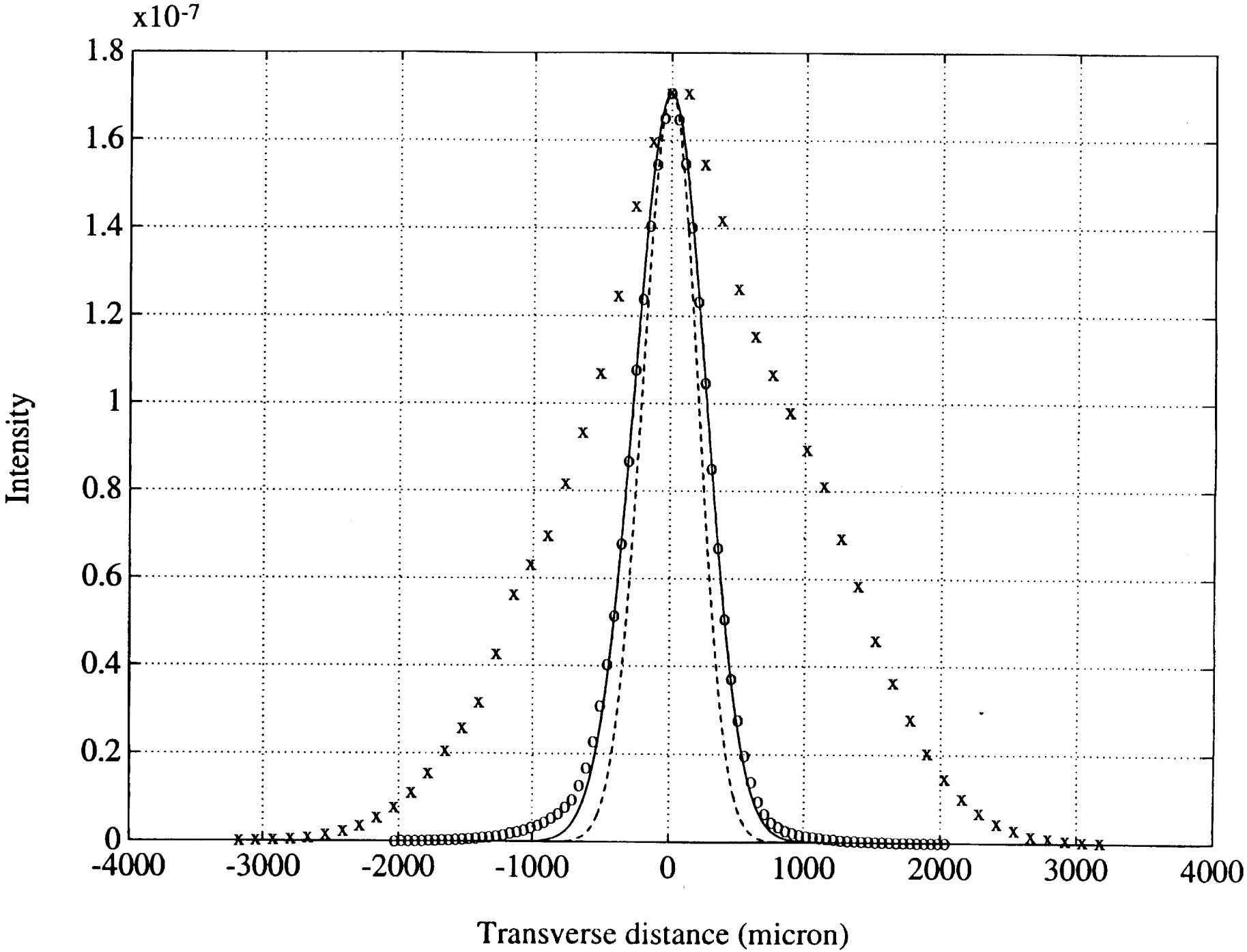
x10-7
1.8
1.6
1.4
1.2
1
0.8
0.6
0.4
0.2
0
Intensity
-4000
-3000
-2000
-1000
0
1000
2000
3000
4000
Transverse distance (micron)

Fig 8b

Compact backscatter fiber optic systems for submicroscopic particle sizing

Harbans S. Dhadwal, Kwang Suh and Romel R. Khan

State University of New York
Department of Electrical Engineering
Stony Brook, New York 11794-2350

N/S

ABSTRACT

A compact backscatter fiber optic system, comprising a semiconductor laser diode, a fiber optic probe and a self-contained photomultiplier, is described. Backscatter fiber optic probes provide easy access over a range of scattering angles between 95 and 175 degrees. Accuracy of the portable dynamic light scattering system is assessed through measurements made on a 39 nm polystyrene latex spheres suspension.

INTRODUCTION

Dynamic light scattering (DLS) is a non-invasive and extremely sensitive technique, which is routinely used for characterization of molecular changes in physiological, polymer, chemical, and colloidal systems[1]. DLS characterizes the temporal fluctuations of laser light scattered by a system of particles undergoing Brownian motion or by a random fluctuations in the refractive index of solutions. Temporal information is retrieved through a measurement of the time autocorrelation of the scattered light, which, in a self-beating experiment, must be collected within a single coherence solid angle[2]. Spatial coherence requirement is a coupled function of the spectral characteristics of the optical source and the three dimensional scattering volume. Spatial coherence considerations for efficient self-beating dictates that the scattered light be collected over a small solid angle (typically, 0.1°). A conventional DLS system comprises a coherent light source (typically Argon ion laser), a high precision goniometer, sample cell holder, bulk optics for beam delivery and detection, a photomultiplier and digital correlator. Such systems, however, are confined to the laboratory environment, and many potentially useful areas of application are deprived of the extremely sensitive technique of DLS. The interested reader is referred to Chu's textbook[3] dealing with the theory and practice of laser light scattering.

The utility and versatility of fiber optics in DLS has been established over the past decade[4-17]. Ansari et al[17] have discussed the recent developments of backscatter fiber optic probes (BFOP). Early BFOP utilized a single optical fiber for transmitting and receiving optical energy to and from the scattering region, and as such are homodyne receivers. The recent BFOP use two optical fibers for separating the transmitting and receiving paths. In this manner these BFOP

are self-beating receivers with several advantages over homodyne systems; the most important being the ability to position the BFOP outside the scattering cell. Characteristics of BFOP have been studied under various conditions and for various systems, however, all previous work used a He-Ne laser source and a photomultiplier requiring a separate high voltage power supply.

The purpose of this paper is to report results obtained by using semiconductor laser diodes (SLD) and a smaller photomultiplier with its built-in high voltage power supply. In this configuration, the DLS system is compact and portable, and may be used for monitoring particle size distributions in an industrial/clinical environments. SLD have been used for DLS[12], but not in a system configuration described in this paper.

THEORETICAL BACKGROUND

DLS involves illumination of the scattering system by a coherent optical source, which is, typically, focused to a 100 μm diameter spot. The scattering volume, formed by the intersection of the effective field of view of the detector system, is controlled so as to maximize the self-beating efficiency, which has to be sacrificed for increased signal strength. The scattered light is converted into a series of photo-electron pulses, which after suitable amplification and discrimination, are correlated, in real time, using a state-of-art digital correlator. The resulting intensity-intensity autocorrelation $G^{(2)}(t_m)$, is related to the first order autocorrelation $g^{(1)}(t_m)$ through the Siegert relation

$$G^{(2)}(t_m) = A\left[1 + \beta|g^{(1)}(t_m)|^2\right] \qquad (1)$$

where A is an estimate of the baseline, t_m is the delay time of the m'th channel and ß is a measure of the self-beating efficiency, having a maximum value of unity. For a suspension of spherical particles of radius r, the first order autocorrelation is expressed as a Laplace transform of the distribution of diffusion coefficients G(D),

$$|g^{(1)}(t_m)| = \int_{D_{min}}^{D_{max}} G(D)\exp(-Q^2 D t_m)dD \qquad (2)$$

where the Bragg wave number Q is given by

$$Q = \frac{4n\pi}{\lambda_o}\sin\left(\frac{\theta}{2}\right) \qquad (3)$$

n is the refractive index of the suspension, λ_o is the free space wavelength, D_{min} and D_{max} are the lower and upper bounds on the diffusion coefficient D, which for spherical particles is expressed through the Stokes-Einstein relation

$$D = \frac{k_B T}{6\pi\eta r}$$

where k_B is Boltzmann's constant, T is the absolute temperature and η is the solution viscosity.

Several techniques are in use for inverting eqns (1) and (2), in order to recover the distribution in particle size. The interested reader should consult the paper by Ross and Dimas[18], in which they discuss the merits of various techniques in use today. For the purpose of analysis in this paper we will use the data inversion software provided the manufacturer of the digital correlator.

FIBER OPTIC SYSTEM

Figure 1 shows a schematic of a backscatter fiber optic system for DLS investigations of particulate solutions. It comprises an electronics module, a fiber optic probe and a data

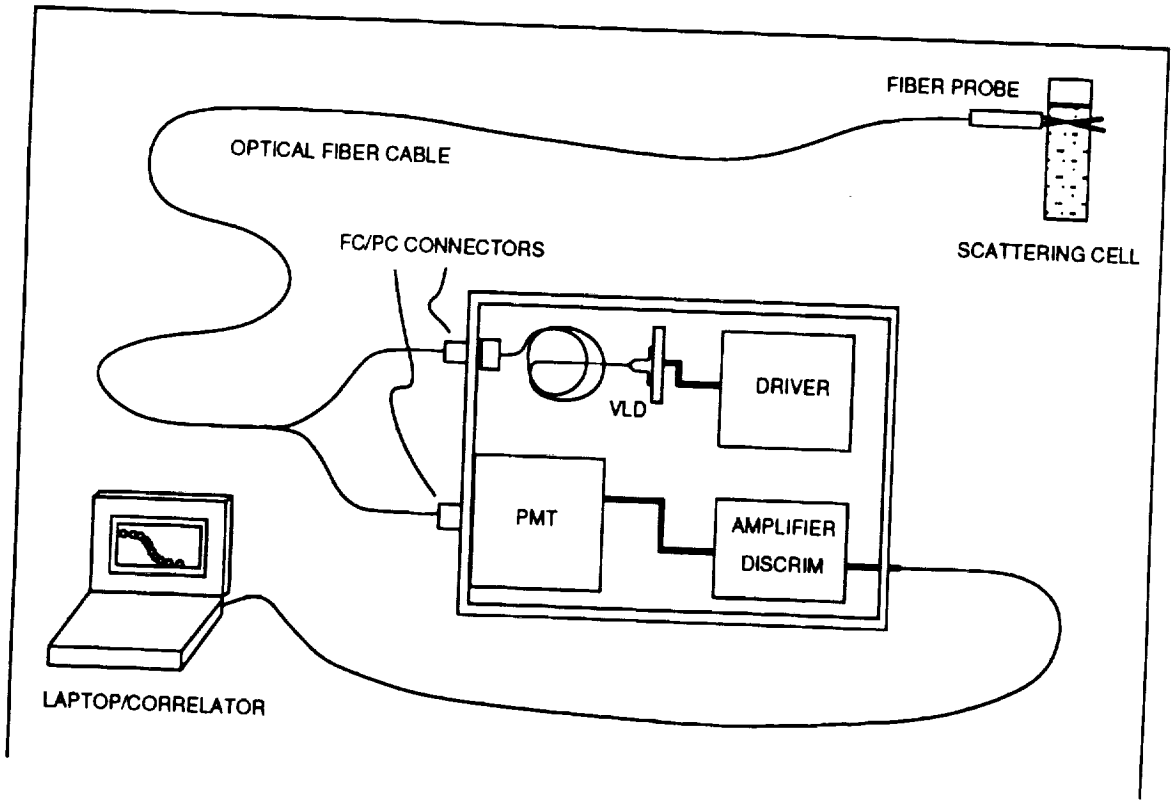

Figure 1: Schematic of a backscatter fiber optic system

acquisition/analysis unit (laptop personal computer with a digital correlator). The system is compact and can be carried in a brief case. BFOP have been used to characterize microemulsions[17], low concentration proteins[15], such as, lysozyme (7.32 mg/ml) and bovine serum albumin (5.50 mg/ml), high concentration proteins[4] found in bovine and human eye lenses and over a wide range of sizes and concentrations of standard polystyrene spheres[5].

The electronics module is designed such that fiber optic probes can be easily interchanged, giving added flexibility to the system; it comprises a pigtailed semiconductor laser, a laser driver, a photomultiplier, an amplifier and discriminator. The output from the electronics module is a random TTL pulse train corresponding to the detection of the scattered photons. The fiber optic probe, described below, can be easily and reproducibly connected to the unit using FC/PC connectors; insertion loss being less than 0.5 dB. The unit is powered from a ±12 volt dc voltage source.

SLD, which are extremely small and require very low electrical power, are replacing conventional laser sources for a variety of applications. Initial development of SLD was fueled by the communications industry, and subsequently resulted in the development of long wavelength SLD. However, in recent years, due to the demand of short wavelength sources for fiber optic sensors, visible laser diodes (VLD) are being developed rapidly. In the present study we have used a VLD (Toshiba model 9215), which is rated to produce 10 mW of optical power at a wavelength of 670 nm. Index guiding ensures a single longitudinal mode with spectral width being less than one tenth of a nanometer.

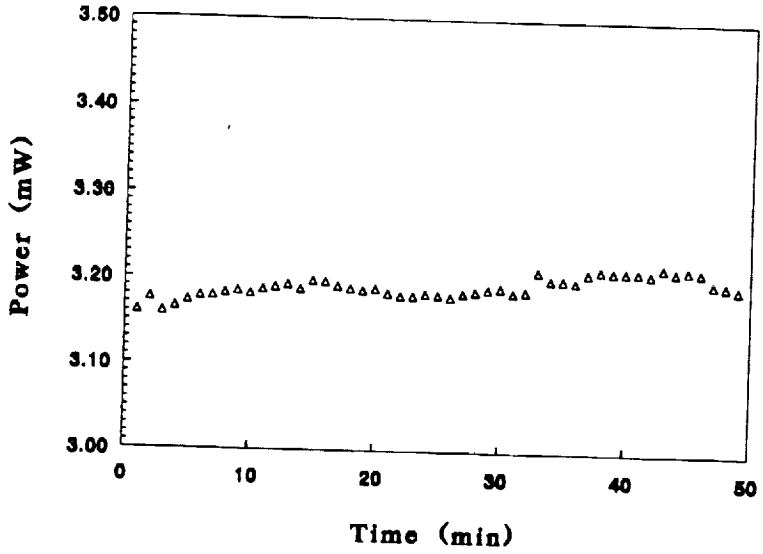

Figure 2: Optical power stability characterization of a VLD, Toshiba model 9215, operating in the constant light mode. Note that the total power is much less than the rated 10 mW for the device, because of the fiber pig-tailing.

A VLD can be operated either in the constant current or constant light mode. The latter mode of operation requires utilization of the built-in monitor photodiode to provide tracking of the output optical power. As shown in Fig. 2, optical power stability, better than 0.5%, can be obtained without the use of temperature control. However, the manufacturer's specify a 0.25 nm change in the peak wavelength for every one degree celsius change in case temperature of the VLD. VLD is an edge emitting structure, which can be characterized by a planar source of dimensions 0.5 by 2 μm. Therefore, the near and far field intensity distributions are highly elliptical. A compact and portable DLS must employ a reliable technique for reproducibly coupling a VLD to the BFOP. As shown in Fig. 1, the VLD is pigtailed to a monomode optical fiber, which is terminated with FC/PC connector. The present state-of-art techniques can couple approximately 50% of the available optical power into the monomode optical fiber. In the system reported here, 4 mW of optical power at a wavelength of 675 nm is available for DLS. This low power output places a lower limit on the size and concentration of particles that can be detected. Coupling to BFOP is achieved through a bulk head adapter, with an insertion loss which is less than 0.5 dB. In this way, different BFOP can be interchanged at will and do not require any alignment.

The scattered photons arrive at the photocathode of a miniature photomultiplier tube (PMT), Hamamatsu model HC-120, via the receiving optical fiber and FC/PC connector. The PMT, which contains a multiplying circuit to generate the necessary high voltage from a low voltage supply, is contained in a package of dimension 12x50x50 mm. Quantum efficiency of this PMT is better than the EMI 9863B PMT, and the dark count, at room temperature, is approximately 30 counts per second. Photoelectric pulses from the PMT, after suitable amplification and discrimination, are correlated using a digital correlator (Brookhaven Instruments model BI8000AT). It should be noted that avalanche photodiodes, having a much higher quantum efficiency, have been used for DLS[12], but as yet no commercial system is available.

Detailed design and fabrication of a fiber optic probe, capable of providing coherent detection of the scattered light in the backward direction, has been discussed elsewhere[4,5,15]. For the purpose of this paper, a typical BFOP, as shown in Fig. 3, comprises two precisely positioned optical fibers, one for transmitting a diverging laser beam to the scattering region and the other for detecting the scattered light. The fiber probe is equivalent to a single angle dynamic light scattering system, although, a multiangle probe has also been fabricated. Careful positioning, both angular and lateral, allows the location and size of the scattering volume to be specified. In the present embodiment the fiber probe provides easy access to scattering species, which may be located in odd shaped scattering cells and/or in remote areas. A fiber probe can be designed to give any scattering angle in the backward direction, and the scattering center can be located up to 5 mm inside the scattering cell.

For the present study we have fabricated two BFOP, which are suitable for DLS measurements at scattering angles of 154° and 94°. The edge of the scattering region is located 4.5 mm from the tip of both probes.

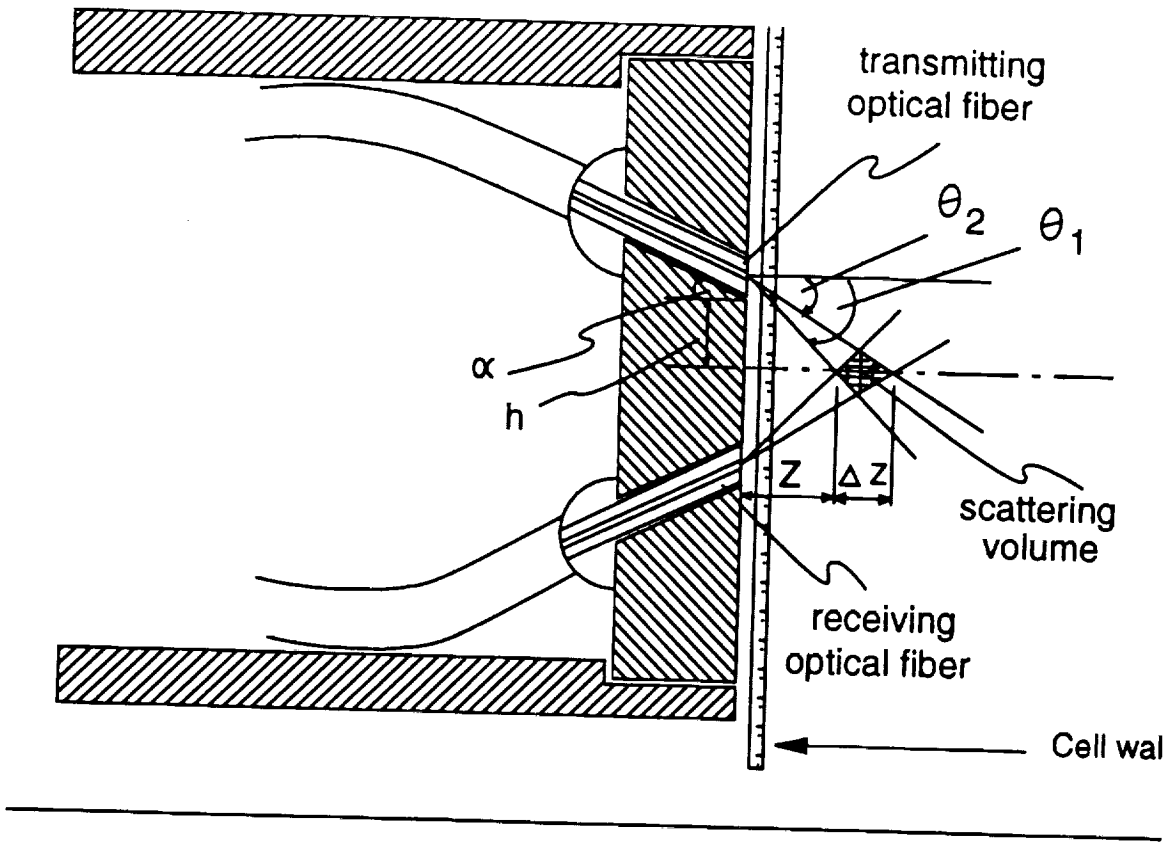

Figure 3: A backscatter fiber optic probe

RESULTS AND DISCUSSION

Polystyrene latex spheres (PLS) with a nominal average diameter of 39 nm were obtained from Bangs Laboratories, Indiana. These aqueous solutions are supplied with a PLS concentration of 10% solids by weight. A sample of 0.05% concentration was prepared using doubly distilled deionized water (18 MΩ resistance). To avoid presence of undesirable dust, final preparations were filtered with a 0.2 μm millipore membrane filter. Samples were transferred to precleaned 10-mm cuvettes.

The system shown in Fig. 1 was used to make measurements on the PLS sample described above using both BFOP. The 154° BFOP was used to measure a series of one hundred autocorrelations, each of 120 second duration. Fig. 4 shows a typical intensity-intensity autocorrelation obtained with the 154°; triangles represent measurements made using a VLD and the diamonds represent measurements made a He-Ne laser source. We note that the self-beating efficiency, ß, obtained with a VLD is close to that obtained with a He-Ne laser, indicating the spectral purity of the VLD. The one hundred autocorrelations were analyzed using a fourth order cumulant analysis; the variation in the average particle diameter obtained from different runs is shown in Fig. 5. The average particle diameter, based on 100 measurements, is 41.4±0.4.

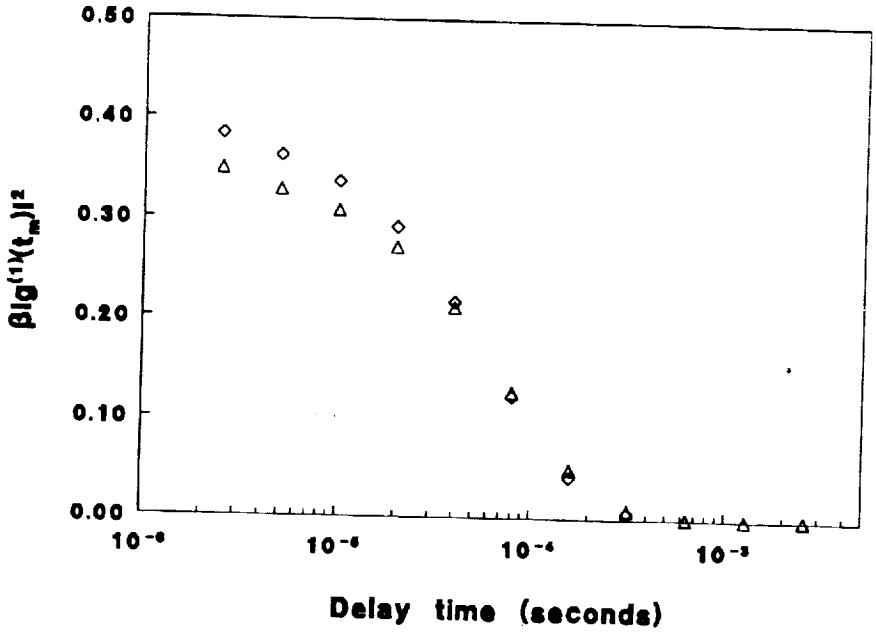

Figure 4: Intensity-intensity autocorrelation obtained using the 154° BFOP from a 0.05% by weight suspension of PLS. triangles - VLD; diamonds - He-Ne model 120.

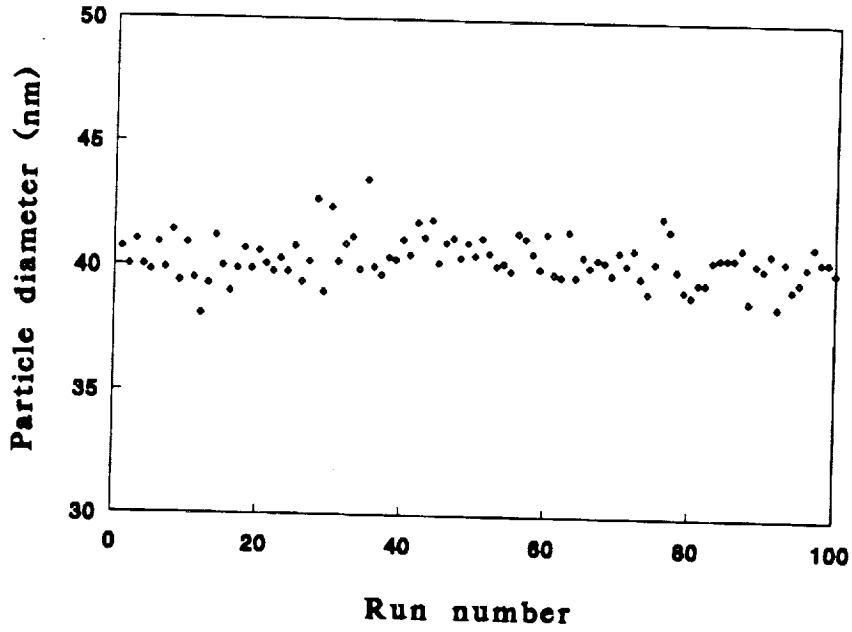

Figure 5: Variation in the particle diameter recovered from autocorrelation using a fourth order cumulant analysis.

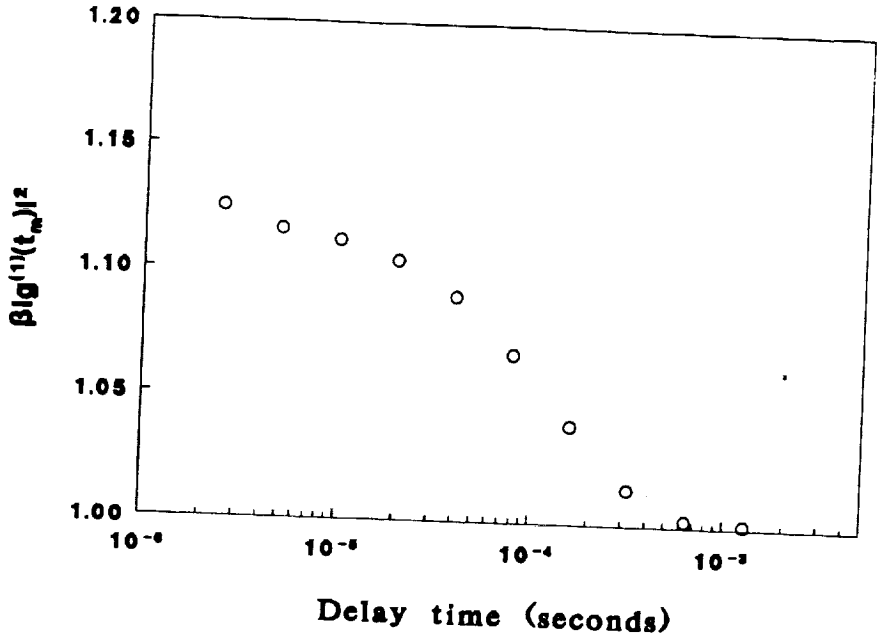

Figure 6: Intensity-intensity autocorrelation obtained using the 94° BFOP

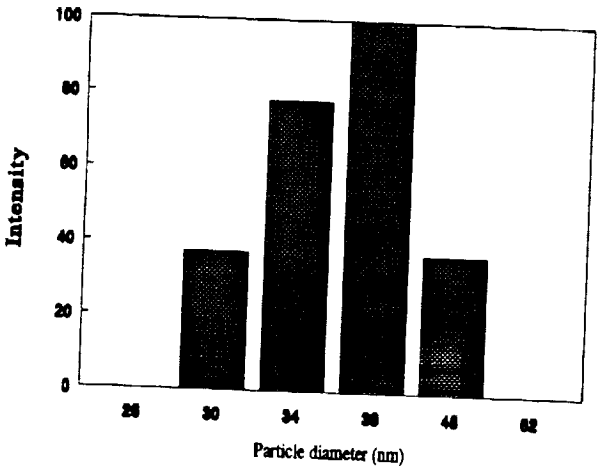

Figure 7: Particle size distribution

Figure 6 shows the intensity-intensity autocorrelation obtained using the 94° BFOP. As expected the self-beating efficiency is lower than that obtained with the 154° BFOP. This is primarily due the distorted incident laser beam spot. However, despite the low self-beating efficiency, it is still possible to recover the distribution in particle diameter, as shown in Fig. 7.

CONCLUSION

In this paper we have described a very compact, rugged and portable fiber optic system, which can provide DLS measurements over a range of scattering angles in the backward direction. The many advantages of fiber optics will permit the use of DLS techniques in a process control environment.

ACKNOWLEDGEMENTS

HSD wishes to acknowledge support from NASA's Microgravity Sciences and Applications Division, code SN, under contract number NCC3-241.

REFERENCES

1. H.S.Dhadwal and B.Chu,"A Fiber Optic Laser Light Scattering Spectrometer", Review of Scientific Instruments, vol. 60, pp.845-853 [also published in SPIE Milestone Series. Vol. MS 12, "Selected Papers on Laser Light Scattering by Macromolecular, Supramolecular and Fluid Systems,"edited by B.Chu (1990)

2. H.S.Dhadwal and B.Chu,"Fiber Optics in Laser Light Scattering Spectroscopy",J. Colloid and Interface Science, vol. 115, pp.561-563 (1987)

3. B. Chu, "Laser Light Scattering: Basic Principles and Practice," Academic Press, New York (1991)

4. Harbans S. Dhadwal, Rafat R. Ansari and Michael A. DellaVecchia, "A Coherent Fiber Optic Sensor For Early Detection of Cataractogenesis in a Human Eye Lens", Optical Engineering:special issue on Biomedical Engineering, vol. 32, 233-238 (1993)

5. Harbans S. Dhadwal, Rafat R. Ansari and William V. Meyer, "A fiber optic probe for particle sizing in concentrated systems," Review of Scientific Instruments, 63, 2963-2968 (1991)

6. H.S.Dhadwal, C.Wu and B. Chu,"Fiber Optic Detector Probes For Laser Light Scattering", Applied Optics,28, 4199-4205 (1989)

7. Rafat R. Ansari, Harbans S. Dhadwal, H.M.Cheung, and William V. Meyer, "Microemulsion characterization using a fiber optic probe", Photon Correlation and Scattering: Theory and Applications, Eighth Topical Meeting, Boulder, Colorado, August 24-26, 1992

8. Harbans S. Dhadwal, Romel Khan and Kwang Suh, "An integrated fiber optic probe for photon correlation spectroscopy", Photon Correlation and Scattering: Theory and Applications, Eighth Topical Meeting, Boulder, Colorado, August 24-26, 1992

9. Rafat R. Ansari, Harbans S. Dhadwal, Michael A. Dellavecchia and Melanie Campbell ,"A fiber optic sensor for ophthalmic refractive diagnosis," Proceeding of the International Society of Optical Engineering: Fiber Optic Medical and Fluorescent Sensors and Applications, Los Angeles, 19-24 January 1992, vol. 1648, pp.83-105

10. Harbans S. Dhadwal and Rafat R. Ansari,"A multiple fiber optic probe for several applications," Proceeding of the International Society of Optical Engineering: Fiber Optic and Laser Sensors IX, vol. 1584, pp 262-272; Boston, MA; 3-6 September 1991

11. Harbans S. Dhadwal "A Back Scatter Fiber Optic Probe For Particle Sizing," Gradient-Index Optical Systems, 1991, Technical Digest Series (Optical Society of America, Washington, DC, 1991), pp.165-167

12. R.G.W. Brown, "Dynamic light scattering using monomode optical fibers," App. Opt., vol. 26, 4846-4849 (1987)

13. D.A.Ross, H.S.Dhadwal and R.B.Dyott, "The determination of the mean and standard deviation of the sized distribution of a colloidal suspension of submicroscopic particles using the fibre optic Doppler anemometer, FODA," J. Colloid and Interface Sci., vol. 64, 533-542 (1978)

14. Auweter and D. Horn, "Fibre-optical quasi-elastic light scattering studies of concentrated dispersions," J. Colloid and Interface Sci., vol 105, 399-409 (1985)

15. Harbans S. Dhadwal, William W. Wilson, Rafat R. Ansari, and William V. Meyer, "Dynamic light scattering studies of BSA and lysozyme using a backscatter fiber optic system," Proceeding of the International Society of Optical Engineering: Fiber Optic Medical and Fluorescent Sensors and Applications, (SPIE, Bellingham, Washington, 1993)

16. H.S. Dhadwal, R.R. Khan and K. Suh, "An integrated fiber optic probe for dynamic light scattering", App. Opt., vol. 32, 3901-3904 (1993)

17. R. R. Ansari, H.S.Dhadwal, H. M. Cheung, and W. V. Meyer, "Microemulsion characterization using a fiber optic probe'" App. Opt. **32**, 3822-3827 (1993)

18. D.A. Ross and Nicholas Dimas, "Particle sizing by dynamic light scattering: Nois and distortion in correlation data," Particle and Particle System Characterization, **10**, 62-69 (1993)

a reprint from Applied Optics

Integrated fiber optic probe for dynamic light scattering

Harbans S. Dhadwal, Romel R. Khan, and Kwang Suh

An integrated fiber optic probe, comprising a monomode optical fiber fusion spliced to a short length of a graded-index multimode fiber, is fabricated for use as a coherent receiver in dynamic light scattering. The multimode fiber is cleaved to provide a gradient-index fiber lens with a focal length of 125 μm and an *f*-number close to unity. An integrated fiber receiver is used to measure the intensity–intensity autocorrelation data from a 0.05% by weight concentration of an aqueous suspension of polystyrene latex spheres. Analysis of 100 independent data sets indicates that the particle size can be recovered with an accuracy of ±1%.

Key words: Graded-index fiber lens, photon correlation spectroscopy, particle sizing, light scattering.

1. Introduction

In the past three decades following the invention of the laser, dynamic light scattering (DLS) has become an indispensable, noninvasive, and extremely sensitive technique for routine characterization of molecular changes in physiological, chemical, polymer, and colloidal systems.[1] DLS involves measurement of the intensity–intensity correlation of the laser light scattered from particles illuminated by a monochromatic light source, followed by a data inversion procedure that yields the distribution of particle sizes. In order to observe the modulation imparted by the particles undergoing Brownian motion, the scattered light must be collected over a well-defined coherence solid angle, which is a function of the size of the scattering volume and wavelength of the light source.[2]

Spatial coherence consideration for efficient self-beating dictates that the scattered light be collected over a small solid angle, typically 0.1°. Figure 1 shows a schematic of detection optics, typically used in commercial instruments to achieve the above uncertainty in the scattering angle. Detection optics comprises a convex lens, two apertures that define uncertainty angle $\Delta\theta$, and the size of the scattering volume. The components are mounted into a cylindrical housing of ~7 cm in diameter and 15 cm in length and attached directly onto the face plate of a photomultiplier. The entire assembly is positioned on a goniometer system, providing access to a range of scattering angles. In the past decade there has been considerable interest in miniaturizing the DLS apparatus through the use of fiber optics. Macfadyen and Jennings provide a review on this subject.[3] A brief review of backscatter fiber optic probes is given by Ansari *et al.*[4]

In this paper we describe the design, fabrication, and utility of an integrated fiber receiver for use in DLS. Detailed designs of these integrated fiber systems has been presented earlier.[5] In this embodiment the fiber receiver, a single integral unit comprising two dissimilar fibers, can be designed to meet any imaging requirement. The integrated fiber probe has no apertures, no air path from the front surface to the detector, and is rugged and extremely compact.

2. Theoretical Background

Figure 2 shows a schematic of a fiber optic receiver, comprising a monomode optical fiber and a quarter-pitch graded-index multimode fiber lens (GFL), integrated together by means of fusion splicing.

By using the eikonal equation,[6] it can be shown that pitch P of a graded-index fiber with a refractive-index profile of the form

$$n^2(r) = n_0^2[1 - (g_0 r)^\Gamma] \tag{1}$$

is given by

$$P = \frac{2n_0' N_0 b^{(1/\Gamma - 1/2)}}{\Gamma n_0 g_0^{\Gamma/2}} \int_0^{2\pi} \sin^{(2/\Gamma - 1)}(\theta) d\theta, \tag{2}$$

The authors are with the Department of Electrical Engineering, State University of New York, Stony Brook, New York, 11794-2350.

Received 1 October 1992.
0003-6935/93/213901-04$06.00/0.

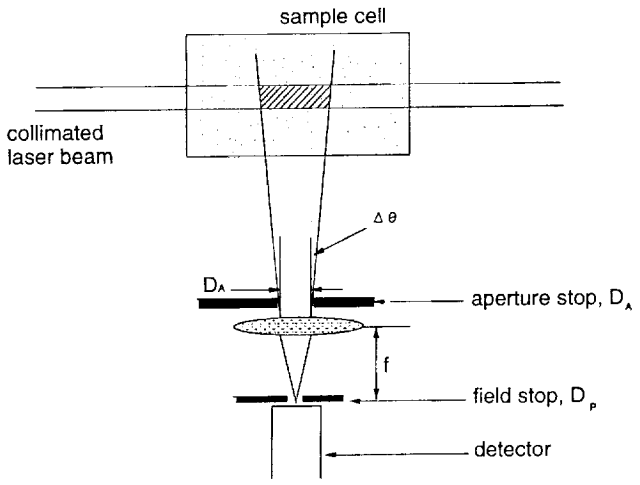

Fig. 1. Schematic of conventional detector optics, nonimaging, $\Delta\theta = D_p/(2f)$.

where r is the radial distance from the optical axis, n_0 is the on-axis refractive index, g_0 is the quadratic index constant, N_0 is the direction cosine of the incident ray with respect to the z axis (bounded by the critical acceptance angle of the optical fiber), n_0' is the refractive index at the incident point, and $b = (n_0^2 - n_0'^2 N_0^2)/(g_0^\Gamma n_0^2)$. For the type of optical fiber considered in this paper, Γ, which is dependent on the material properties and wavelength, is approximately 2.0.

In the first-order approximation, Eq. (2) reduces to

$$P \approx \frac{2\pi}{g_0}. \tag{3}$$

Length L of the fiber lens is related to the fractional pitch η by

$$L = 2\pi\eta/g_0. \tag{4}$$

It can be shown that, for a quarter-pitch fiber lens, effective aperture D_A and uncertainty angle $\Delta\theta$ are given by[5]

$$D_A = \frac{2\lambda}{g_0 n_0 \pi w_0}, \tag{5}$$

$$\Delta\theta = g_0 n_0 w_0, \tag{6}$$

where w_0 is the core radius of the monomode fiber.

In Table 1 we compare typical values of D_A and $\Delta\theta$ for the conventional system shown in Fig. 1, for the Dhadwal and Chu fiber probe,[2] and for the integrated fiber probe discussed above. Table 1 also shows a comparison of the relative sizes of the detection optics.

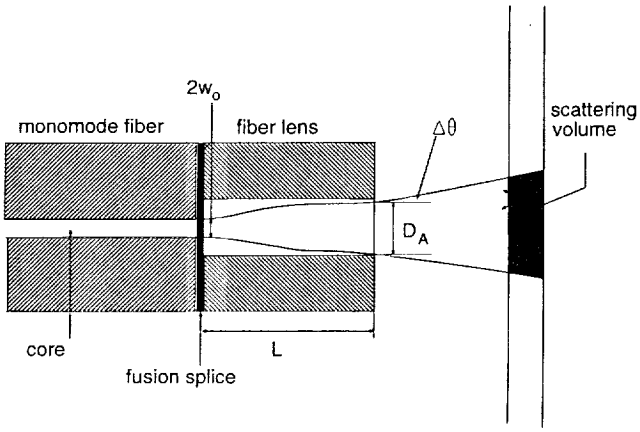

Fig. 2. Integrated fiber optic receiver with a quarter-pitch fiber lens.

3. Experimental Procedure

A. Fabrication of an Integrated Coherent Fiber Receiver

A fiber receiver, as described above, was fabricated by using a monomode optical fiber (Newport model F-SV) with a core radius $w_0 = 2$ μm and a multimode optical fiber (Newport model F-MSD) with a core diameter of 50 μm, $g_0 = 5.46$ mm^{-1} and $n_0 = 1.465$. The two fibers were integrated together by using a fusion splicer (Power Technology model PFS200). Active alignment was used for precise positioning of the two fibers. Fusion splice parameters such as current and duration are determined experimentally for any pair of fibers being spliced. For the particular case reported here we used a prefuse current of 17 mA for a duration of 0.3 seconds, followed by a fuse current of 17 mA for a duration of 1.2 s. Typical values of splice loss and strength, as quoted by the manufacturer, are 0.15 dB and 1.4 GN/m^2, respectively. The Fresnel loss at the splice point is considerably smaller than the loss of the fiber–air interface. We have not observed any instabilities in the laser light emanating from the fiber tip.

The critical step in the process of fabricating a fiber probe is the ability to cleave the multimode fiber to the desired length. This procedure is performed under an optical microscope (total magnification ≈500). The spliced fiber is mounted onto a differential micrometer (Newport model DM13) stage (Newport model M425) that is held onto a microscope stage assembly together with a mechanical cleaver (Fujikura model CT-04). The fusion point is located under the microscope and aligned with the scribing rotary blade. The fused fiber is pulled back to the

Table 1. Comparison of the Receiver Effective Diameter, Uncertainty Angle, and Size for a Conventional System, Dhadwal and Chu's Gradient-Index Probe,[2] and an Integrated Fiber Optic Probe

Detector Type	D_A (μm)	Δθ (deg)	Size
Conventional system (Fig. 1)	500	0.06	75 mm × 150 mm
Gradient-index microlens probe[2] (monomode fiber + SLS 2.0 lens)	500	0.05	4.0 mm × 40 mm
Integrated fiber probe (monomode fiber + 0.23P fiber lens)	25	1.2	250 μm × 300 μm

desired length by the differential micrometer and then cleaved. By means of the procedure, we can cleave and then measure the length of the GFL within an accuracy of ± 6 μm. This accuracy is limited by the inability to locate the splice point precisely, as a good fusion splice is difficult to locate under the microscope. Additionally there is some uncertainty in matching the cleaving position with the position of the scribing rotary blade. A GFL for the integrated probe reported here was cleaved to a length of $0.23P$.

The integrated fiber probe was characterized by launching a He–Ne laser beam into the unlensed end of the fiber and measuring the optical radiation pattern emanating from the lensed end of the monomode fiber. Figure 3 shows the far-field intensity distribution at a distance of 8 mm from the tip of fiber (circles). The solid curve represents the expected distribution for a $0.23P$ fiber lens, based on Gaussian imaging.[5] The dashed curve shows the intensity distribution for a quarter-pitch fiber lens, and the crosses show the experimental intensity distribution for an unlensed monomode fiber. From Fig. 3 we can ascertain that our integrated fiber receiver has an effective diameter of $D_A = 25$ μm and an uncertainty angle $\Delta\theta = 1.2°$. Certainly in conventional systems we would not use such a large uncertainty in the scattering angle; however, we were limited by the choice of available multimode fibers.

B. Sample Preparation

Polystyrene latex spheres (PLS's) with a nominal average diameter of 85 nm (lot L890612C) were obtained from Bangs Laboratories, Indiana. These aqueous solutions are supplied with a PLS concentration of 10% by weight. A sample of 0.05% concentration was prepared by using doubly distilled deionized water (18-MΩ resistance). To avoid the presence of undesirable dust, final preparations were filtered with a 0.2-μm millipore membrane filter. Samples were transferred into precleaned 10-mm cuvettes.

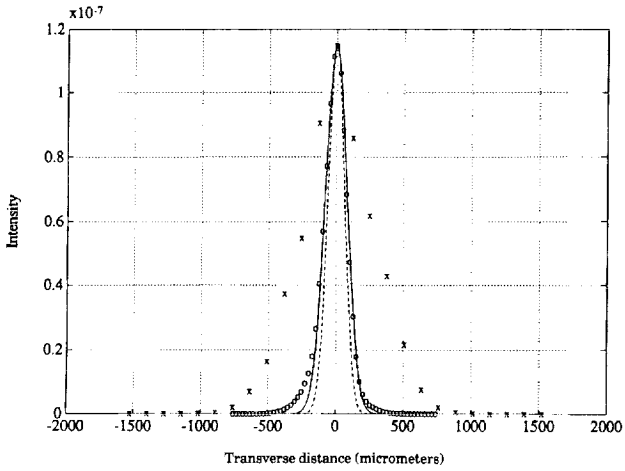

Fig. 3. Characterization of the far-field intensity distribution for an integrated fiber receiver with a $0.23P$ fiber lens: o, measured data points at distance of 8 mm from tip; solid curve, expected distribution; dashed curve, expected distribution for a $0.25P$ lens; x, measured data from an unlensed monomode fiber at an 8-mm distance.

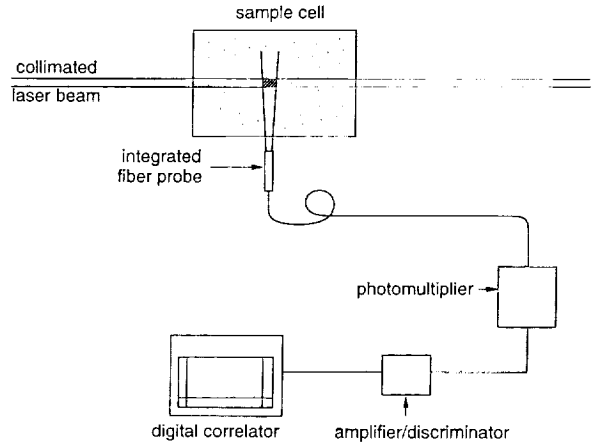

Fig. 4. Schematic of the experimental apparatus for DLS.

C. Experimental Setup

A schematic of the experimental apparatus is shown in Fig. 4. An unfocused, collimated laser beam from a 5.0-mW He–Ne laser (Spectra Physics model 120S) was directed through the sample solution. The fiber optic receiver was positioned at a scattering angle of 90° and ~8 mm from the scattering center. The unlensed end of the monomode fiber was connected to a photomultiplier (Hamamatsu model HC120). Photoelectron pulses, after suitable amplification and discrimination, were fed into a digital correlator (Brookhaven Instrument, Inc., model BI8000AT) to obtain measurement of the intensity–intensity autocorrelation. Subsequent analysis of the autocorrelation yielded the particle size distribution. Data analysis procedures have been discussed at length by many authors, and we do not reproduce them in this paper. The reader is referred to Chu's textbook[7] for additional information.

Figure 5 shows a typical normalized intensity–

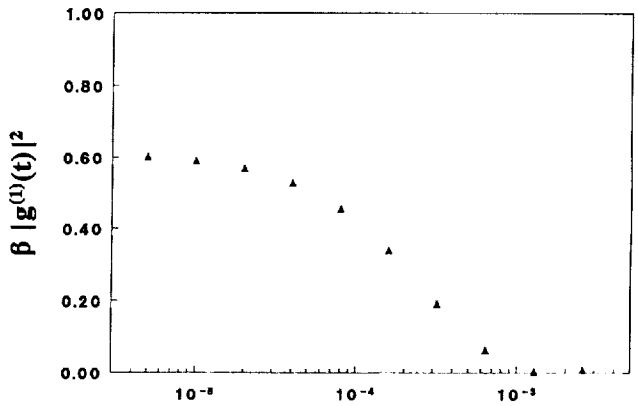

Fig. 5. Normalized intensity autocorrelation $\beta|g^{(1)}(t)|^2$ obtained from an aqueous suspension of 85-nm PLS by the use of the integrated fiber receiver. β is the spatial coherence factor, $g^{(1)}(t)$ is the first-order field autocorrelation, and t is the delay time.

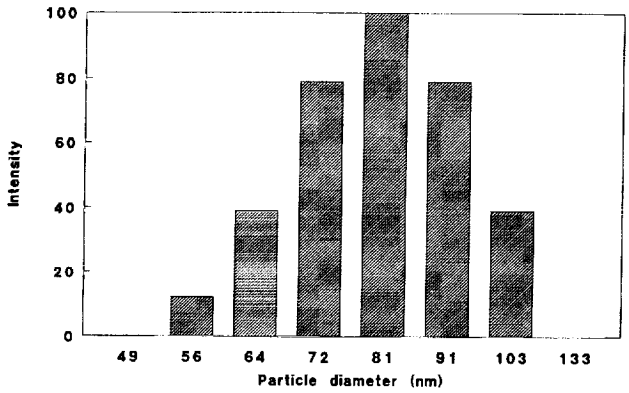

Fig. 6. Size distribution obtained from the inversion of the data in Fig. 5 by the use of a nonnegative least-squares data inversion technique.

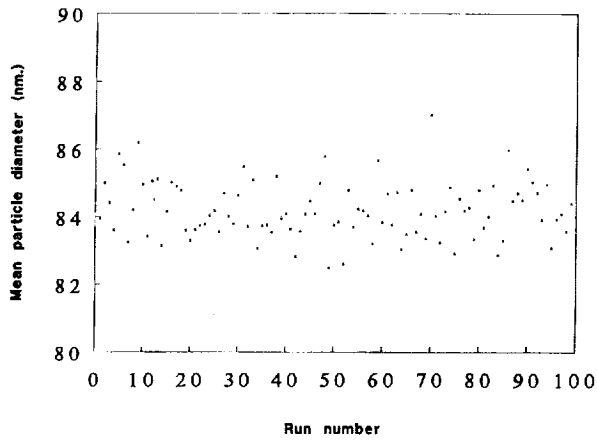

Fig. 7. Accuracy of particle size estimation by the use of an integrated fiber optic receiver. Each data point represents an independent estimation of the particle diameter from an intensity autocorrelation.

intensity autocorrelation obtained from the PLS sample at room temperature. It should be noted that β, a measure of the self-beating efficiency, is a little low because of the use of an unfocused laser beam and the large uncertainty angle $\Delta\theta = 1.2°$. The dependence of β on the size of the scattering volume was discussed by Dhadwal and Chu.[2] Figure 6 shows the corresponding particle size distribution obtained by the use of the nonnegative least-squares inversion procedure supplied by the manufacturers of the correlator. In order to assess the accuracy of the particle size measurements, 100 autocorrelations, each of 60-s duration, were recorded and analyzed by the use of a third-order cumulant analysis.[8] Figure 7 shows a plot of the nominal diameter as a function of the run number. The average diameter is computed to be 84.2 ± 0.8 nm, which is within 1% of the expected 85 nm. As expected, the polydispersity parameter was 0.002 ± 0.003, indicating an extremely narrow distribution.

4. Summary

In this paper we have described the fabrication of an integrated fiber optic receiver and demonstrated its utility for DLS. An integrated fiber optic probe has no apertures, requires no adjustment, and can have an overall diameter as small as 250 μm. Error in the determination of the particle diameter of PLS was within the theoretical limit of $\pm 1\%$, corresponding to an uncertainty in the scattering angle of 1.2°.[9]

The authors are grateful to William Emkey for permitting access to the fusion splicer and to Curtis Jack for his assistance and patience in using the splicer. H. Dhadwal acknowledges the continuous support from NASA Lewis Research Center under contract NCC3-241.

References

1. B. Chu, ed. *Quasielastic Light Scattering by Macromolecular, Supramolecular, and Fluid Systems,* Vol. MS12 of SPIE Milestone Reprint Series (Society of Photo-Optical Instrumentation Engineers, Bellingham, Wash., 1990).
2. H. S. Dhadwal and B. Chu, "A fiber-optic light scattering spectrometer," Rev. Sci. Instrum. **60,** 845–853 (1989).
3. A. J. Macfadyen and B. R. Jennings, "Fiber optic systems for dynamic light scattering—a review," Opt. Laser Technol. **22,** 175–187 (1990).
4. R. R. Ansari, H. S. Dhadwal, H. M. Cheung, and W. V. Meyer, "Microemulsion characterization using a fiber optic probe," Appl. Opt. **32,** 3822–3827 (1993).
5. H. S. Dhadwal, R. R. Khan and K. Suh, "Integrated coherent imaging fiber optics," presented at the Tenth Topical Meeting on Gradient-Index Optical Systems, Santiago de Compostela, Galicia, Spain, 1992.
6. T. Okoshi, *Optical Fibers* (Academic, New York, 1982), Chap. 2, pp. 42–43.
7. B. Chu, *Laser Light Scattering* (Academic, New York, 1991), Chap. 7, pp. 243–280.
8. E. Koppel, "Analysis of macromolecular polydispersity in intensity correlation spectroscopy: the method of cumulants," J. Chem. Phys. **57,** 4814–4820 (1972).
9. H. S. Dhadwal, R. R. Ansari, and W. V. Meyer, "A fiber-optic probe for particle sizing in concentrated suspensions," Rev. Sci. Instrum. **62,** 2963–2968 (1991).

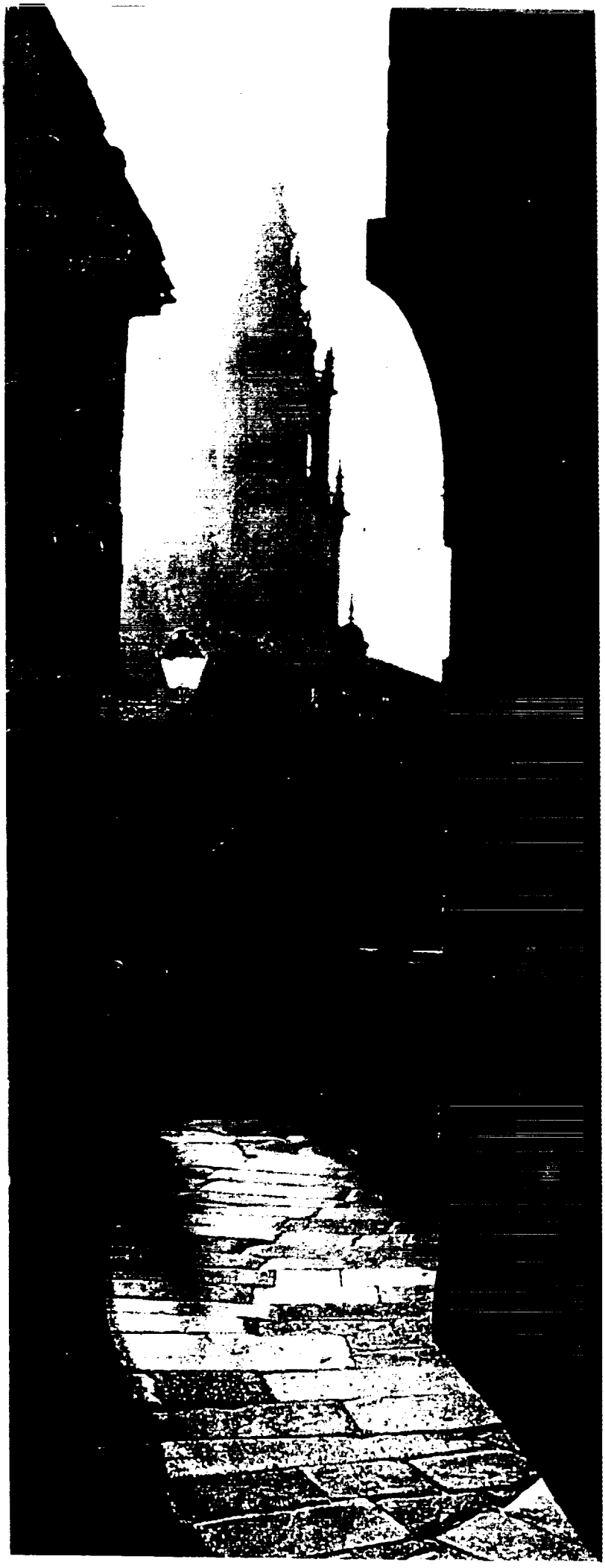

Grin 92

Santiago de Compostela
GALICIA · SPAIN
4-6 OCTOBER 1992

NIS

Tenth Topical Meeting on
GRADIENT-INDEX OPTICAL SYSTEMS

Organized by
University of Santiago de Compostela

In Cooperation with
European Optical Society (EOS)
Japan Society of Applied Physics (JSAP)
Optical Society of America (OSA)
Optical Society of Spain (SEDO)
Telefónica I+D (Spain)

TECHNICAL DIGEST

INTEGRATED COHERENT IMAGING FIBER OPTICS

Harbans S. Dhadwal, Romel R. Khan and Kwang Suh
State University of New York
Department of Electrical Engineering
Stony Brook, New York 11794-2350, USA

SUMMARY

Delivery of a narrow collimated coherent light beam has been a long sought goal in photon correlation spectroscopy (PCS), particularly for the characterization of physiological, polymer and chemical systems. Conventional apparatus employing bulk optics have been replaced by graded index and fiber optics, resulting in considerable miniaturization and ruggedness[1]. High power densities in the measurement volume, achieved by means of focussing, are necessary for probing weakly scattering systems. A collimated beam of diameter less than 100 μm would be desirable, however, commercial collimating fiber pigtails give a beam diameter in excess of 1000 μm.

In this paper, we report the design and fabrication of an integrated fiber optic probe, comprising of a monomode optical fiber, which is fusion spliced to a short length of a graded index multimode fiber, for delivery of either a collimated beam with diameter less than 50 μm or a focussed spot to a remote location. Variation in the image distance and magnification is obtained by controlling the length of the fiber lens for a fixed object to lens distance. Emkey and Jack[2] evaluated such lenses in connection with the development of low loss fiber optic connectors.

Figure 1 shows a schematic of a generic integrated coherent fiber optic probe. Using the eikonal equation[3], it can be shown that the pitch P, of a fiber having a refractive index profile of the form

$$n^2(r) = n_0^2(1-(g_0 r)^{\Upsilon}) \qquad (1)$$

is given by,

$$P = \frac{2n_0' N_0 b^{(1/\Upsilon - 1/2)}}{\Upsilon n_0 g_0^{\Upsilon/2}} \int_0^{2\pi} \sin^{(2/\Upsilon - 1)}(\theta)\, d\theta \qquad (2)$$

where r is the radial distance from the optical axis, n_0 is the on-axis refractive index, g_0 is the quadratic index constant, N_0 is the direction cosine of the incident ray with respect to z-axis (bounded by the critical acceptance angle of the optical fiber), n_0' is the refractive index at the incident point, Υ is in the range 2.0 to 2.2 for the fibers considered here, and $b = \frac{n_0^2 - n_0^2 N_0^2}{g_0^{\Upsilon} n_0^2}$.

We note that a multimode graded index optical fiber has focussing properties similar

to those of conventional lenses and SELFOC[4] graded index lenses manufactured by NSG[4]. The imaging conditions are dependent upon the choice of the length L, which is expressed as a fraction of the pitch P. For example, L=0.25P results in a fiber lens which has the front and back focal planes coincident with the end surfaces. Such a fiber lens is ideal for mating to a monomode optical fiber to produce a collimated output. The two fibers can be integrated together by means of fusion splicing; thereby, eliminating the interface and resulting in a robust collimator, with negligible insertion loss.

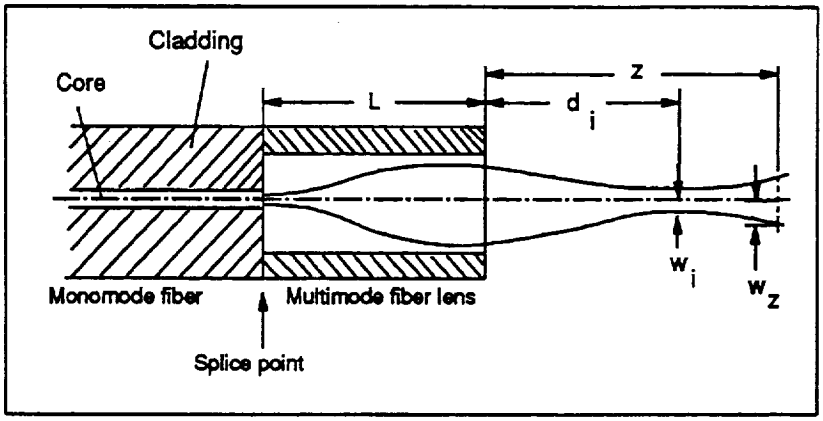

Figure1: Schematic of an integrated imaging fiber optic probe

The optical field distribution radiating from the tip of a monomode fiber can be approximated by a gaussian profile having a beam waist w_0, corresponding to the core radius of the monomode fiber, which is fusion spliced to the front surface of the multimode fiber as shown in figure 1. The image beam waist w_i, and position d_i are given by[5]

$$\frac{w_i}{w_0} = \frac{1}{[(\frac{g_0 \sin(2\pi\eta)}{a})^2 + \cos^2(2\pi\eta)]^{1/2}} \tag{3}$$

$$d_i = \frac{\sin(4\pi\eta)[g_0^2 - a^2]}{2n_0 g_0[g_0^2 \sin^2(2\pi\eta) + a^2\cos^2(2\pi\eta)]} \tag{4}$$

where $\eta = \mathrm{L}/P$ and is in the range 0 to 1.0, and $a = \frac{\lambda}{\pi n_0 w_0^2}$.

Figures 2(a) & 2(b) show plots of the image distance d_i and magnification (w_i/w_0) as a function of η, respectively. We can see that for η=0.25 we obtain the largest beam diameter but the least divergence. Based upon these calculations, several imaging fiber probes were fabricated using a fusion splicer. Figure 3 shows a comparison of the experimental and theoretical results obtained for one such probe. A monomode fiber, Newport model FSV, w_0=2 μm, was fusion spliced to a multimode fiber, Newport model MSD, having η=0.33. Laser light from a He-Ne laser, Melles Griot model GLG5261, was launched into the free

end of the monomode fiber by means of a x20 microscope objective. A fiber coupled to a power meter, Newport model 835, was used to record the transverse intensity distribution at various positions, z, from the tip of the imaging probe. Figure 3(a) shows a comparison of the intensity distribution from an unlensed monomode fiber (crossmarks) and the imaging probe (circles) at z=15.3 mm. Theoretical prediction for the intensity distribution at z, in the paraxial limit, is given by

$$I_z = I_0 \exp(-\frac{2r^2}{w_z^2}) \tag{5}$$

where

$$w_z^2 \simeq w_0^2\{[\cos(2\pi\eta) - n_0 z g_0 \sin(2\pi\eta)]^2 + a^2[\frac{\sin(2\pi\eta)}{g_0} + n_0 z \cos(2\pi\eta)]^2\}$$

Figure 3(b) shows a comparison of the expected intensity distribution (solid line) at z=15.3 mm and experimental results (circles). The dashed line is the expected distribution for a 1/4-pitch fiber lens. Figure 3(c) and (d) are at z=33.1 mm, showing similar agreement between theory and experiment.

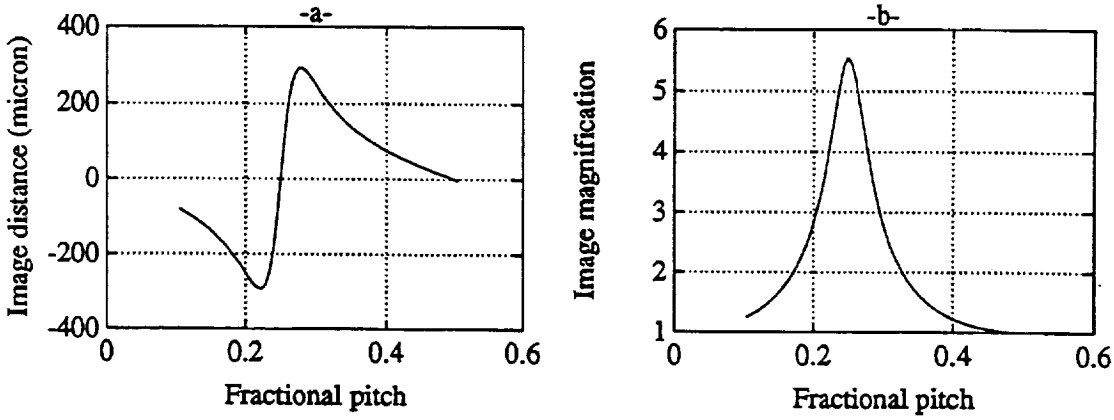

Figure 2. Theoretical plot for the imaging properties of the integrated fiber optic probe. (a) equation 3, and (b) equation 4, with ω_0=2 μm, g_0=6.21 mm^{-1}, n_0=1.465, and λ=0.633 μm.

In conclusion, we have described the design and fabrication of an integrated fiber optic imaging probe. Experimental results have been in close agreement with theoretical expectations. Such probes can be customized for a variety of diverse applications.

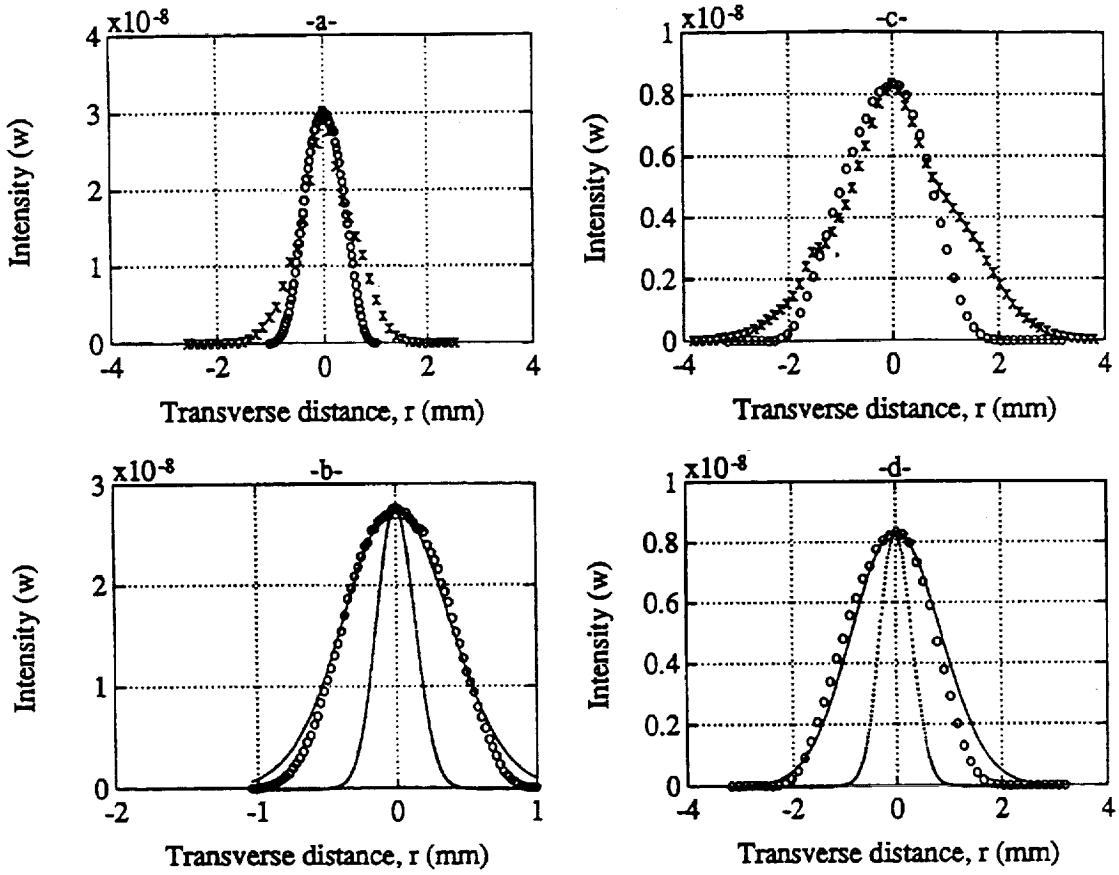

Figure 3. Experimental results for an unlensed monomode fiber(x) and an integrated fiber probe(o) at (a)z = 15.3 mm, and (c)z = 33.1 mm. Theoretical plots: solid line (η=0.33), and dashed line (η =0.25), and experimental result(o) for (b)z = 15.3 mm, and (d)z = 33.1 mm.

REFERENCES

1. Benjamin Chu, *Laser Light Scattering*, Academic Press, New York (1991)
2. Emkey and Jack, "Analysis and Evaluation of Graded-index fiber lenses", Journal of Lightwave Technology, Vol. LT-5, Sep. 1987, 1156-1164.
3. Takanori Okoshi,*Optical Fibers*, Chap 2 & 3, Academic Press, New York (1982).
4. SELFOC is a trademark of Nippon Sheet Glass Company.
5. Acosta, Flores, Gómez-Reino and Liñares,"Gradient index lens law for Gaussian illumination: image and focal shifts",Optical Engineering, Nov. 1989, Vol. 28, 1168-1172.

ACKNOWLEDGEMENT

Authors are very thankful to Dr. William Emkey for allowing access to the fusion splicer, and to Curtis Jack for his patience and assistance in using the splicer.

Microemulsion characterization by the use of a noninvasive backscatter fiber optic probe

Rafat R. Ansari, Harbans S. Dhadwal, H. Michael Cheung, and William V. Meyer

This paper demonstrates the utility of a noninvasive backscatter fiber optic probe for dynamic light-scattering characterization of a microemulsion comprising sodium dodecyl sulfate/1-butanol/brine/heptane. The fiber probe, comprising two optical fibers precisely positioned in a stainless steel body, is a miniaturized and efficient self-beating dynamic light-scattering system. Accuracy of particle size estimation is better than ±2%.

Key words: Dynamic light scattering, fiber optic sensors, particle sizing, microemulsions, fuels, quasi-elastic light scattering.

1. Introduction

A. Microemulsions

Microemulsions are clear, thermodynamically stable dispersions of two immiscible liquids with carefully adjusted emulsifiers (surfactants and cosurfactants). The cosurfactants are normally short chain alcohols. The globule size of the dispersed phase is normally less than 1 μm. Oil-in-water, bicontinuous, and water-in-oil (W/O) microemulsion systems can be obtained on changing the solution environment by altering salinity or the concentration of a surfactant.[1,2]

One difficulty in studying critical microemulsions has been stratification[2] and hydrodynamic instabilities[3] that are due to gravity. This gravity sensitivity is not completely unexpected as there are experimental[4–7] and theoretical[8,9] indications that the very low free energy differences between states with significantly different microstructures can lead to substantial composition variations in microemulsions, especially in the middle phase. Further, microdroplet clustering is believed to precede phase separation in some cases,[10] leading to local density differences between the disperse and the continuous phases on a length scale large enough to promote stratification. The physical–chemical state of the microemulsions remains a subject of discussion because of questions of polydispersity and shape of the droplets, surface properties of the electrically charged droplets in ionic systems, droplet–droplet interactions, the effect of pH on phase behavior, and the role of the interfacial film because of surfactants and cosurfactants.

One of the most sought-out physical characteristics of a microemulsion system is the globule size in the case of a monodisperse system and the globule size distribution in the case of a polydisperse system. The expected size range is in the submicrometer regime, and therefore dynamic light scattering (DLS) techniques are very appropriate for experimental characterization of microemulsions.[1] There are many textbooks on the subject of light scattering and the interested reader should consult Ref. 11 for a historical perspective of the subject and Ref. 12 for understanding the practice of DLS.

B. Review of Backscatter Fiber Optic Systems

The first backscatter fiber optic system, a fiber optic Doppler anemometer (FODA), was described by Dyott in 1978.[13] The FODA was successfully developed into a compact and portable single-angle DLS system for use in the sizing of colloidal suspensions[14,15] and for the routine characterization of the motility of bovine spermatozoa.[16] The FODA represented a significant break from conventional DLS systems by enclosing the transmitting and the receiving optics into a T-shaped metal housing, which was mounted directly onto a helium neon laser. Transmitted and scattered laser light was guided to and from the

R. R. Ansari and W. V. Meyer are with NASA Lewis Research Center/Case Western Reserve University, Mail Stop 105-1, 21000 Brookpark Road, Cleveland, Ohio 44135-3191. H. S. Dhadwal is with the Department of Electrical Engineering, State University of New York at Stony Brook, Stony Brook, New York 11794-2350. H. M. Cheung is with the Department of Chemical Engineering, The University of Akron, Akron, Ohio 44325-3906.

Received 30 September 1992.
0003-6935/93/213822-06$06.00/0.

scattering region through a single multimode optical fiber. Separation of the transmitted and scattered signals was achieved by means of a hole-in-mirror beam splitter mounted into the T-shaped housing. The FODA provided a homodyne detection of the scattered light in the backward direction (180° ± 4.5°). The local oscillator was derived from the phase mismatch at the fiber–liquid interface. The FODA successfully demonstrated the utility of fiber optics for making DLS accessible to clinical–industrial environments. Additionally, the free end of the fiber was dipped directly into the scattering system, consistent with clinical–industrial requirements, as demonstrated in the measurements carried out on bovine spermatozoa for the artificial insemination program.[17]

Auweter and Horn[18] modified the FODA by replacing the hole-in-mirror beam splitter with a multimode fiber optic directional coupler. In 1991, Dhadwal[19] reported a backscatter fiber optic probe, which utilized separate optical fibers for transmitting and receiving, thereby eliminating the need for a beam splitter. Homodyne detection was achieved through the use a gradient-index microlens positioned in contact with two fibers, which were placed side by side. As discussed by Dhadwal *et al.*[20] and Thomas,[21] the single-fiber backscatter systems (homodyne) exhibit unreliability and ambiguity in the estimation of size from concentrated suspensions; this arises because of the lack of knowledge of the relative strength of the local oscillator to scattered signal strength. In order to overcome this difficulty, a more efficient and compact backscatter fiber optic probe, which provided a self-beating detection of the scattered light, was developed.[20] The self-beating fiber optic probe comprises two optical fibers positioned side by side, but mounted into a common ferrule. The fiber probe was designed for direct immersion into the scattering medium. The accuracy and reliability of this probe was demonstrated over a range of aqueous concentrations of several different standards of polystyrene latex spheres (PLS's). Dhadwal and Ansari[22] also developed another type of self-beating backscatter fiber optic probe, which provided simultaneous access to a range of scattering angles in the backward direction. In particular, a linear array of fibers was positioned in the back focal plane of a gradient-index microlens. One of the fibers was used for delivering a Gaussian laser beam to the scattering region, while the remaining fibers provided access to 10 backscatter angles separated by 2.2°.

There are many potential applications that could benefit from the use of a backscatter fiber optic probe, but require noninvasive interrogation. Single-fiber backscatter systems (homodyne) are not suitable for positioning outside sample containers, but the self-beating probe, comprising two separate optical fibers, can be modified for this purpose. As shown in Fig. 1, the two optical fibers, in addition to being displaced in the transverse direction, can also be tilted with

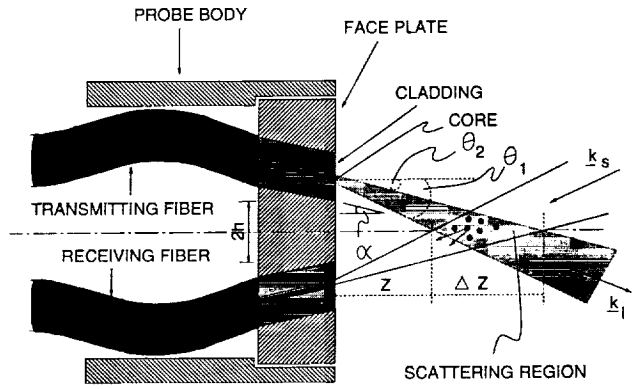

Fig. 1. Schematic of a noninvasive lensless backscatter fiber optic probe. θ is the scattering angle, k_I and k_s are the incident and scattering wave vectors, respectively; $|k_I| = |k_s| = 2\pi/\lambda_0$, where λ_0 is the free-space wavelength of the laser source.

respect to each other. This added degree of freedom allows precise location of the edge of the scattering region from the tip of the probe body, thereby enabling the fiber probe to be positioned outside the scattering cell. With this added feature, the backscatter fiber optic probe provides access to odd-shaped and remotely located scattering cells. We have successfully applied the noninvasive backscatter probe to the study of cataractogenesis in excised but intact human[23] and bovine[24] eye lenses, and low molecular weight protein systems in the dilute regime.[25]

In this paper we demonstrate the utility and the effectiveness of a noninvasive fiber probe to perform DLS study on a microemulsion system. This preliminary investigation establishes the important role of noninvasive backscatter fiber optic probes. A typical microemulsion system is characterized by several phases, and the precise location of each phase may not always be known *a priori*. In order to study the dynamics of such systems by the use of DLS, an optical apparatus with the capability of interrogating the stratified column, without disturbing the microemulsion, is required. A conventional DLS system with distributed and bulky transmitted and receiving optics, would require considerable modification to meet this challenge. In contrast, a noninvasive backscatter probe, as described below, is ideally suited for such applications.

2. Noninvasive Backscatter Fiber Optic Probe

The requirements of a noninvasive backscatter fiber optic probe are more demanding than those of an immersible filter probe. The noninvasive fiber probe must illuminate and interrogate a small volume in the interior region of a scattering vessel while providing self-beating detection; strong backreflections from the scattering vessel must not enter the receiving fiber. Figure 1 shows a schematic of a lensless noninvasive backscatter fiber probe body, which consists of a cylindrical stainless steel tube with a matching faceplate. Two optical fibers are epoxied into precisely drilled holes in the face plate. Separation h and inclination α between the two holes define

scattering angle θ, and edge of the scattering region Z, from the fiber probe tip and the length of the scattering region ΔZ. One of the fibers is used for illuminating the scattering region with a diverging Gaussian laser beam, while the second optical fiber, together with a photomultiplier connected to the other end of the fiber, provides a self-beating detection of laser light scattered in the backward direction.

The challenge in the design of a backscatter fiber optic probe lies in determining the optimum pair of values for h and α that provide acceptable estimates of particle size from the measured intensity–intensity autocorrelation data and that are consistent with required values of Z and ΔZ. Assuming that the two optical fibers are identical, the following set of equations, which governs the design of the fiber probe, can be derived by geometric arguments:

$$Z = \left[h + \frac{D_f}{2\cos(\alpha)}\right]\frac{1}{\tan(\theta_1)}, \quad (1)$$

$$\Delta Z = \left[h + \frac{D_f}{2\cos(\alpha)}\right]\left[\frac{1}{\tan(\theta_2)} + \frac{1}{\tan(\theta_1)}\right], \quad (2)$$

$$\theta = \pi - 2\sin^{-1}[(n_1/n_2)\sin(\alpha)], \quad (3)$$

$$\sin(\theta_1) = (n_1/n_2)\sin(\alpha + \rho), \quad (4)$$

$$\sin(\theta_2) = (n_1/n_2)\sin(\alpha - \rho), \quad (5)$$

$$\rho = \cos^{-1}(n_3/n_1), \quad (6)$$

where D_f is the core diameter of the optical fiber; θ_1 and θ_2 are determined by the numerical aperture of the optical fiber and the refractive index of the scattering medium n_2; and n_1 and n_3 are the refractive indices of the core and the cladding of the optical fiber, respectively. From the above set of equations, it can be ascertained that a self-beating, lensless, and noninvasive fiber optic probe can be designed to meet a range of challenging experimental conditions. For example, it is possible to fabricate a fiber probe capable of providing measurements of the scattered light at 90°, without the use of any other optical components. From the above equations, we have fabricated a backscatter lensless fiber optic probe with a nominal scattering angle of 143° in aqueous solutions, $Z \approx 3$ mm, and $\Delta Z < 1$ mm. The waist of the Gaussian laser beam exiting from the fiber probe has a waist radius of 2 μm. It is appropriate to note at this point that there may be some applications for which delivery of a focused laser beam is critical. This issue is discussed by Dhadwal *et al.*[26] in a paper in this feature issue. That paper discusses the integration, through fusion splicing, of a gradient-index fiber lens to a monomode optical fiber, before it is mounted into the faceplate. The process of fusion splicing and subsequent cleaving is still being perfected.

3. Experimental Procedure

A. Sample Preparation

Our experiments employed a three-phase microemulsion system comprising sodium dodecyl sulfate (SDS)/1-butanol/brine/heptane. Details on this system can be found elsewhere.[27] SDS (98%), 1-butanol [99.9+%, high-performance liquid chromatography (HPLC) grade], n-heptane (99+%, HPLC grade), and NaCl [99.9+%, American Chemical Society reagent grade) were obtained from Aldrich Chemical Company and, aside from filtering stock solutions, were used as received. Water was de-ionized and filtered (0.2 μm) as supplied and was again thrice filtered (0.2 μm) before use. Samples were prepared from 20 wt. % SDS and NaCl stock solutions, heptane, water, and 1-butanol. The SDS and NaCl stock solutions and water were thrice filtered through a 0.2-μm filter to remove dust. The heptane and 1-butanol were used as received. The HPLC-grade 1-butanol and n-heptane were filtered by the manufacturer (0.5 μm). The A-series microemulsions consist of equal weight fractions of a 6.54 wt. % NaCl brine and n-heptane and varying percentages of a surfactant mixture. The surfactant mixture is composed of SDS and 1-butanol in the mass ratio 1:2. The compositions are provided in mass percent in Table 1. The samples were prepared in 13-mm Kimax screw-cap test tubes that had been repeatedly rinsed with thrice-filtered (0.2-μm) water and then dried. The sealed samples were equilibrated for a minimum of 24 h before use.

B. Experimental Setup

The experimental setup, which is described elsewhere,[20] requires coupling of light into the transmitting monomode optical fiber and a photomultiplier for the detection of photons collected by the receiving optical fiber. A 20× microscope objective was used to couple light from a He–Ne laser source (NEC Model GLG 5261), with a peak power of 5 mW, to the monomode optical fiber. Optical power emanating from the probe tip was adjusted to ~ 1 mW in order to establish a lower threshold for operation of the fiber probe DLS system. Figure 2 shows a photograph of the fiber probe interrogating a microemulsion column.

Table 1. Composition of A-Series Microemulsion Samples

Sample	Surfactant Mixture	6.54 wt. % NaCl Solution	Heptane
A0	1.00	49.50	49.50
A1	3.00	48.50	48.50
A2	5.00	47.50	47.50
A3	7.00	46.50	45.50
A4	9.00	45.50	45.50
A5	11.00	44.50	44.50
A6	13.00	43.50	43.50
A7	15.00	42.50	42.50
A8	17.00	41.50	41.50
A9	20.00	40.00	40.00

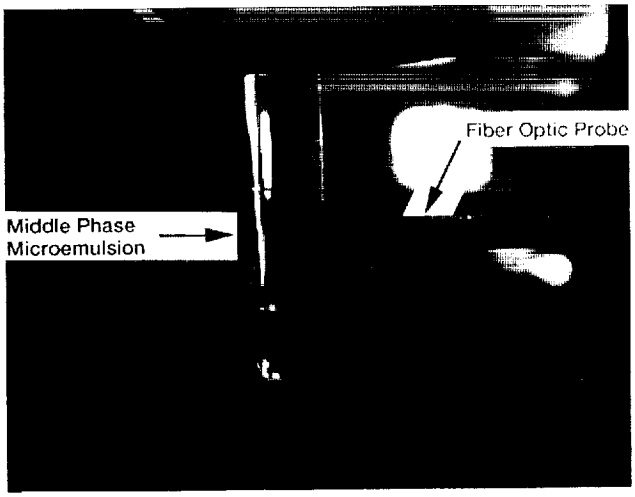

Fig. 2. Photograph showing the fiber probe interrogating the microemulsion system.

A conventional DLS system (Brookhaven Instruments Corporation Model BI-2000SM), operating at a wavelength of 514.5 nm with a power level of 400 mW, was used to make measurements of the intensity–intensity autocorrelation on the same set of samples. Photoelectron pulses from either the fiber system or the BI-200SM were correlated with a digital correlator (Brookhaven Instruments Corporation Model BI2030). Intensity–intensity autocorrelation data from 10 microemulsion samples were measured for a 300-s duration with both systems discussed above.

C. Data Analysis

In a typical DLS experiment the measured intensity–intensity autocorrelation $G^{(2)}(t_m)$, and the normalized first-order electric-field autocorrelation $g^{(1)}(t_m)$, are related through the Siegert relation,

$$G^{(2)}(t_m) = A[1 + \beta|g^{(1)}(t_m)|^2], \tag{7}$$

where A is an estimate of the baseline, t_m is the delay time of the mth channel, and β is a measure of the self-beating efficiency, with a maximum value of unity.

The first-order electric-field autocorrelation is given by a Laplace transform of the distribution of diffusion coefficients $G(D)$, that is,

$$\sqrt{\beta}g^{(1)}(t_m) = \left[\frac{G^{(2)}(t_m)}{A} - 1\right]^{1/2} = \sqrt{\beta}\int_{D_{\min}}^{D_{\max}} G(D)\exp(-Q^2Dt_m)\mathrm{d}D, \tag{8}$$

where $Q = (4n\pi/\lambda_0)\sin^2(\theta/2)$ is the Bragg wave number, n is the refractive index of the suspension medium, λ_0 is the free-space wavelength of the coherent light source, θ is the scattering angle, and $D_{\min}$ and $D_{\max}$ are the lower and upper bounds, respectively, on the diffusion coefficient D. The diffusion coefficient is related to radius r of spherical particles through the Stokes–Einstein equation,

$$D = \frac{kT}{6\pi\eta r}, \tag{9}$$

where k is Boltzmann's constant, T is the absolute temperature, and η is the solvent viscosity.

Data analysis involves inversion of the Laplace transform expressed in Eq. (8) to obtain $G(D)$, or a characteristic linewidth distribution $G(\Gamma)$, with $\Gamma = Q^2D$. This inversion procedure is ill conditioned in the presence of noise, which is unavoidable in the accumulation of data. Many techniques for solving this inversion problem are in existence. The reader is referred to Chu's textbook[12] for a detailed account of these procedures. Subsequent to obtaining $G(\Gamma)$, the particle size distribution can be recovered through a scaling process involving Eq. (9) and knowledge of the scattering amplitude for each of the species in suspension.

The autocorrelation data in this paper has been analyzed by the use of a cumulant expansion of the kernel in Eq. (8), as described by Koppel,[28] and by the use of a nonnegative least-squares technique, as described by Lawson and Hanson.[29]

4. Results and Discussion

An aqueous suspension of PLS's (obtained from Bang Laboratories) with nominal diameters of 85 nm and a weight concentration of 0.05% was prepared as described in Ref. 26. Ten 60-s duration intensity–intensity autocorrelations were measured by the fiber probe system and analyzed by a third-order cumulant analysis.[28] The results, summarized in Table 2, show that the accuracy of recovering the particle diameter is better than ±2%. Additionally, as expected, the overall polydispersity factor is fairly small, and the nominal self-beating factor is 0.86.

Table 2. Summary of the Third-Order Cumulants Analysis of Autocorrelation Data Obtained From 0.05% by Weight Concentration Polystyrene Latex Spheres of 85-nm Nominal Diameter[a]

Run Number	β	Particle Diameter (nm)	Polydispersity
1	0.86	87.4	0.005
2	0.86	85.7	0.005
3	0.86	89.2	0.005
4	0.87	86.3	0.005
5	0.86	88.4	0.005
6	0.87	85.6	0.055
7	0.87	85.9	0.067
8	0.86	87.9	0.005
9	0.86	87.3	0.005
10	0.86	85.1	0.005

[a]These measurements were taken with the fiber probe system. Polydispersity is a measure of the ratio of the standard deviation to the square of the mean.

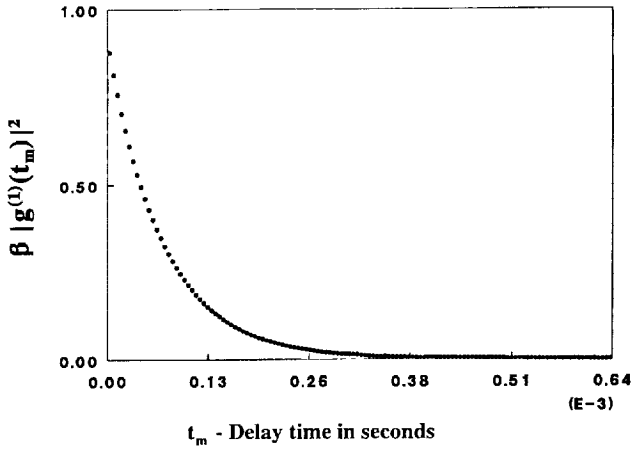

Fig. 3. Normalized intensity–intensity autocorrelation function obtained from the lower phase microemulsion (sample A3). $g^{(1)}(t_m)$ is the first-order electric-field autocorrelation, t_m is the time of the mth delay channel, and β is the self-beating efficiency factor.

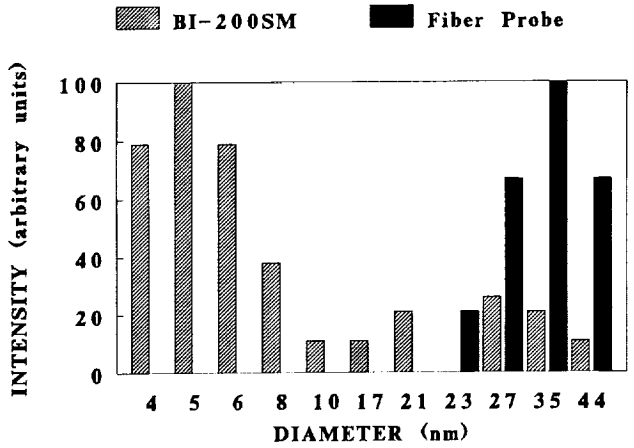

Fig. 5. Comparison of the particle size distributions recovered, by the use of a nonnegative least-squares curve fitting,[29] from a concentrated dispersion (10 wt. %) of 39-nm PLS's. Both measurements were made at a scattering angle of 143°.

The 10 samples of microemulsion classified in Table 1 were characterized by the use of both the backscatter fiber optic probe and the BI-200SM system. Figure 3 shows a normalized intensity–intensity autocorrelation we obtained from sample A3 using the fiber probe. We used a third-order cumulant analysis to analyze the autocorrelation data obtained from all 10 samples. Figure 4 shows a comparison of the average globule diameter of the microemulsion in the various phases. Solid diamonds and solid triangles correspond to data we obtained using the fiber system and the BI-200SM system, respectively. There is good agreement between measurements made in the lower- and middle-phase microemulsions, with the exception of sample A4. Samples A8 and A9, in the upper phase, exhibit differences in the estimates of the globule diameter.

Microemulsions are transparent solutions, but because of their high-volume fractions, they may exhibit multiple light scattering (MLS) effects. In the dispersions of PLS's, MLS effects are pronounced at higher particle concentrations.[20,21] The BI-200SM system gave lower estimates of particle size, consistent with MLS effects.[21] In order to confirm that this discrepancy is due to MLS, we prepared a 10% weight concentration of an aqueous dispersion of PLS's with nominal diameters of 35 nm. Autocorrelation data obtained with both the fiber probe and the BI-200SM were analyzed by a nonnegative least-squares procedure supplied by the digital correlator. Figure 5 shows a comparison of the size distributions recovered from the autocorrelation data. The BI-200SM system was also used at a scattering angle of 143°. As expected,[21] the backscatter fiber probe gives very reasonable estimates of the particle size at these high concentrations. The BI-200SM, as would any other conventional DLS system, gives particle size estimates that are lower than expected. Microemulsion samples A8 and A9, as indicated in Table 1, have high surfactant concentrations of 17 and 20 wt. %, respectively. If we interpret a high surfactant concentration as producing similar effects as a high concentration of PLS, as discussed above, then MLS accounts for the discrepancy between the size estimates shown in Fig. 5.

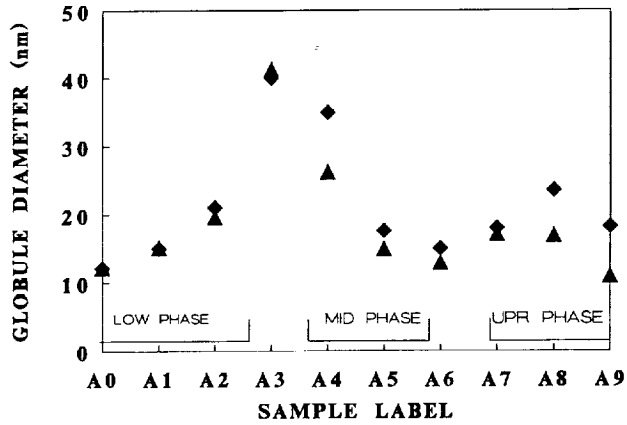

Fig. 4. Characterization of the three-phase microemulsion. Globule diameter is determined by a third-order cumulants analysis[28] of the autocorrelation data. Solid diamonds and solid triangles represent measurements made with the fiber probe and with the BI-200SM system, respectively.

5. Conclusion

In this paper we have used a noninvasive backscatter fiber optic probe to characterize a microemulsion system consisting of SDS/1-butanol/brine/heptane. Our DLS optical system has a unique design that does not require any lenses, has no moving parts, does not need alignment, is insensitive to vibrations, and mitigates the problems of MLS.

The authors thank NASA's Microgravity Sciences and Applications Division, Code SN, and Thomas K. Glasgow of the Processing Science and Technology Branch of the NASA Lewis Research Center for their support of this work. H. S. Dhadwal and H. M.

Cheung acknowledge the research support from grants NCC-3241 and NAG3-906, respectively.

References

1. A. A. Calj'e, W. G. M. Agterof, and A. Vrij, "Light scattering of concentrated W/O microemulsion; Application of modern fluid theories," in *Micellization, Solubilization, and Microemulsions,* K. L. Mittal, ed. (Plenum, New York, 1976), Vol. 2, pp. 779–790.
2. B. Pouligny and F. Nallet, "Free surface instability and stratification of critical microemulsions," Europhys. Lett. **6,** 341–347 (1988).
3. L. Quentela, N. Fernandex, J. Quiben, D. Losada, and C. Ferreiro, "Nonequilibrium phenomena in critical microemulsions," Progr. Colloid Polym. Sci. **76,** 165–168 (1988).
4. J. J. Rosen and Z.-P. Li, "The nature of the middle phase in three-phase micellar systems at phase behavior optimal salinity," J. Colloid Interface **97,** 456–464 (1984).
5. F. Zhao, M. J. Rosen, and N-L. Yang, "Spin probe studies of the microviscosity gradient in the middle phase of three-phase micellar systems," Colloids Surf. **11,** 97–108 (1984).
6. R. J. Good, J. T. Ho, G. E. Groers and X. Yang, "The anomaly of sedimentation at normal gravity in microemulsion," J. Colloid Interface **107,** 290–292 (1985).
7. R. J. Good, J. T. Ho, G. E. Groers, and X. Yang, "Sedimentation in middle phase microemulsions: an investigation using light scattering and ultracentrifugation," Colloids Surf. **20,** 187–209 (1986).
8. Y. Jeng and C. A. Miller, "Theory of microemulsions with spherical drops. I. Phase diagrams and interfacial tensions in gravity free systems," Colloids Surf. **28,** 247–269 (1987).
9. J. Jeng and C. A. Miller, "Theory of microemulsions with spherical drops. II. Effects of gravity," Colloids Surf. **28,** 271–288 (1987).
10. A. M. Ganz and B. E. Boeger, "Fluorescence method for observing clustering of microemulsion droplets near the critical point," J. Colloid Interface Sci. **109,** 504–507 (1986).
11. B. Chu, ed., *Selected Papers on Quasielastic Light Scattering by Macromolecular, Supramolecular, and Fluid Systems,* Vol. MS12 of SPIE Milestone Series (Society of Photo-Optical Instrumentation Engineers, Optical Engineering Press, Bellingham, Wash. 1990).
12. B. Chu, *Laser Light Scattering: Basic Principles and Practice* (Academic, New York, 1991).
13. R. B. Dyott, "The fiber optic Doppler anemometer," Microwave Opt. Acoust. **2,** 13–18 (1978).
14. D. A. Ross, H. S. Dhadwal, and R. B. Dyott, "The determination of the mean and standard deviation of the size and distribution of a colloidal suspension of submicroscopic particles using the fibre optic Doppler anemometer, FODA," J. Colloid Interface Sci. **64,** 533–542 (1978).
15. H. S. Dhadwal and D. A. Ross, "Size and concentration of particles in Syton using the fibre optic Doppler anemometer, FODA," J. Colloid Interface Sci. **76,** 478–489 (1980).
16. D. A. Ross, H. S. Dhadwal, and J. A. Foulkes, "Laser measurement of the motility of bull spermatozoa in an egg yolk diluent," J. Reprod. Fertil. **67,** 263–268 (1983).
17. J. G. Bullock and D. A. Ross, "The measurement of sperm motility by fibre optic Doppler anemometer as prediction of bovine fertility," Lasers Opt. Eng. **4,** 39–53 (1983).
18. H. Auweter and D. Horn, "Fibre-optical quasi-elastic light scattering studies of concentrated dispersions," J. Colloid Interface Sci. **105,** 399–409 (1985).
19. H. S. Dhadwal, "A back scatter fiber optic probe for particle sizing," in *Gradient-Index Optical Systems,* Vol. 9 of 1991 OSA Technical Digest Series, (Optical Society of America, Washington, D.C., 1991), pp. 165–167.
20. H. S. Dhadwal, R. R. Ansari, and W. V. Meyer, "A fiber optic probe for particle sizing in concentrated systems," Rev. Sci. Instrum. **63,** 2963–2968 (1991).
21. J. C. Thomas, "Fiber optic dynamic light scattering from concentrated dispersions. 2. Concentration dependence of the apparent diffusion coefficient," Langmuir **5,** 1350–1355 (1989).
22. H. S. Dhadwal and R. R. Ansari, "A multiple fiber optic probe for several applications," in *Fiber Optic and Laser Sensors IX,* R. P. DePaula and E. Udd, eds., Proc. Soc. Photo-Opt. Instrum. Eng. **1584,** 262–272 (1991).
23. H. S. Dhadwal, R. R. Ansari, and M. A. DellaVecchia, "A coherent fiber optic sensor for early detection of cataractogenesis in a human eye lens," Opt. Eng. **32,** 233–238 (1993).
24. R. R. Ansari, H. S. Dhadwal, M. A. DellaVecchia, and M. Campbell, "A fiber optic sensor for ophthalmic refractive diagnosis," in *Fiber Optic Medical and Fluorescent Sensors and Applications,* D. R. Hansmann, F. P. Milanovich, G. G. Vurek, and D. R. Walt, eds., Proc. Soc. Photo-Opt. Instrum. Eng. **1648,** 83–105 (1992).
25. H. S. Dhadwal, W. Wilson, R. Ansari, and W. V. Meyer, "Dynamic light scattering studies of BSA and Lysozyme using a backscatter fiber optic system," in *Fiber Optic Medical and Fluorescent Sensors and Applications,* D. R. Hansmann, F. P. Milanovich, G. G. Vurek, and D. R. Walt, eds., Proc. Soc. Photo-Opt. Instrum. Eng. **1648** (to be published).
26. H. S. Dhadwal, R. R. Khan, and K. Suh, "Integrated fiber optic probe for dynamic light scattering," Appl. Opt. (to be published).
27. J. Van Nieuwkoop, R. B. De Boer, and G. Snoei, "Microemulsion phase relationships in the system sodium dodecyl sulphate/1-butanol/brine/heptane," J. Colloid Interface Sci. **109,** 350–363 (1986).
28. D. E. Koppel, "Analysis of macromolecular polydispersity in intensity correlation spectroscopy: the method of cumulants," J. Chem. Phys. **57,** 4814–4820 (1972).
29. C. L. Lawson and R. J. Hansen, *Solving Least Squares Problems* (Prentice-Hall, Englewood Cliffs, N.J., 1974).

PROCEEDINGS REPRINT

SPIE–The International Society for Optical Engineering

Reprinted from

Proceedings of

Static and Dynamic Light Scattering in Medicine and Biology

21–22 January 1993
Los Angeles, California

Volume 1884

Dynamic light scattering studies of BSA and lysozyme using a backscatter fiber optic system

Harbans S. Dhadwal, William W. Wilson[1], Rafat R. Ansari[2], and William V. Meyer[2]

State University of New York, Department of Electrical Engineering, Stony Brook, NY 11794-2350

ABSTRACT

A comparative dynamic light scattering study of BSA and lysozyme is presented. A backscatter fiber optic system and a conventional light scattering spectrometer are used to measure the diameter of proteins in the dilute regime, that is, below concentrations of 10 mg/ml. The fiber optic system operating with a power level of 2 mW at a wavelength of 632.8 nm compares favorably with a conventional system operating with a power level of 40 mW at a wavelength of 514.5 nm. Quasi-elastic light scattering measurements taken at several concentrations demonstrate the utility of a backscatter fiber optic probe for sizing of small molecular weight proteins. The fiber probe, comprising two optical fibers, is about 3 mm in diameter and can be positioned either inside or outside the scattering cell.

1. INTRODUCTION

The utility and versatility of fiber optics in quasi-elastic light scattering (QELS) has been established over the past five years[1-11]. The most important features of an optical fiber are its size (core/cladding diameters of 4/125 μm), flexibility and finite numerical aperture. Use of optical fibers, merely as light pipes, is an under utilization of the full potential. By careful choice and design, lens-less fiber optic probes have been constructed for QELS studies of systems ranging from concentrated colloidal suspensions[2] to concentrated protein solutions in excised but in tact eye lenses[1,8], to microemulsions[6]. Fiber probes have been designed to provide a coherent self-beating detection of the scattered light in the backward direction, whereas, all previous backscatter anemometers provided a homodyne detection[12-13]. Fiber probes can be designed to give a self-beating efficiency in the range from zero to unity. Early versions of the fiber probes were fabricated for direct immersion into the scattering medium, thereby eliminating all interfaces between the scattering region and detector. In certain applications, the insertion of the fiber probe into the scattering region is not possible, and may be undesirable. A backscatter probe, constructed for positioning outside the scattering cell, gave very good QELS measurements from excised human eye lenses[1].

One potentially useful application for the QELS backscatter fiber probe is for experiments involving unusually shaped or difficult to access sample containers. An important illustration is found in the area of protein crystal growth where protein solutions are often placed in non-traditional cells of marginal optical quality or even suspended from various surfaces in the so-called hanging drop method. A small diameter backscatter probe would allow measurements on such systems for which traditional methods of laser beam delivery and signal detection are not feasible.

An essential requirement for the DLS backscatter probe is that the proper QELS parameters be determined for relatively weak scatterers such as low molecular weight proteins. The intensity autocorrelations obtained from

[1] Mississippi State University, MS 39762
[2] NASA Lewis Research Center/CWRU, Cleveland, OH 44143

0-8194-1111-6/93/$6.00

the backscatter measurements should not only give reliable estimates for the mean particle size but also for the state of aggregation of the protein solution. In order to test this aspect of the probe, we have conducted measurements on two protein samples, lysozyme and bovine serum albumin, and compared the results with those obtained by traditional QELS methods on the exact same sample.

2. DESIGN CONSIDERATIONS

QELS studies of small molecular weight scatterers in the dilute regime requires careful optimization of the experimental parameters as well as ultra clean sample preparation. As discussed by Ford[14], ideal experimental conditions dictate a highly focussed laser spot in the scattering region and collection of the scattered light in the forward direction. Even under the ideal conditions, the lowest concentration that can be studied is determined by the ratio of scattered intensity from the solute molecules to that from the solvent. According to Ford, the limiting concentration is 0.5 mg/ml for solute molecules of molecular weight 25,000.

Figure 1 shows a schematic of a lens-less backscatter fiber probe body. It comprises of two precisely positioned optical fibers, one for transmitting a diverging laser beam to the scattering region and the other for providing a self-beating detection of the scattered light. Clearly, this configuration contradicts the acceptable guidelines for achieving good QELS results from weak scatterers in the dilute regime. Motivation for pursuing the fiber optic system comes from the possible benefits arising from the ability to position the fiber probe in inaccessible places. The overall diameter of the probe can be as small as 500 μm, however, for ease of handling we used a 3 mm stainless steel tubing for making the first prototype for use in the present study.

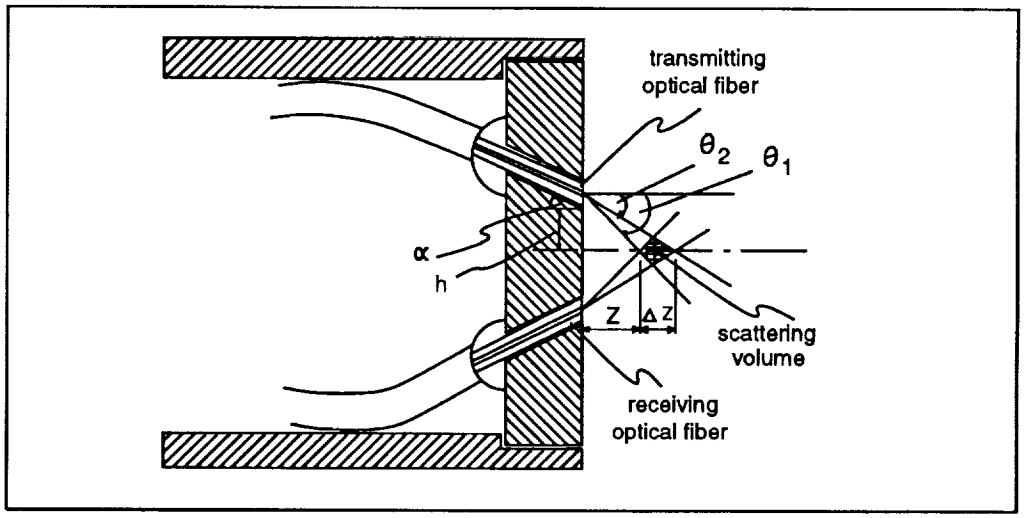

Figure 1: Schematic of a generic backscatter fiber optic probe.

The challenge in the design of a backscatter fiber optic probe is to determine the optimum values of h and α, which would lead to acceptable determinations of the protein size in the dilute regime. The critical issues in the design are the location, z of the edge of the scattering region from the tip of the probe body and the size of the scattering volume ΔZ. Assuming that the two optical fibers are identical it can be shown that,

$$Z = \left[h + \frac{D_f}{2\cos(\alpha)}\right] \frac{1}{\tan(\theta_1)} \tag{1}$$

$$\Delta Z = \left[h + \frac{D_f}{2Cos(\alpha)}\right] \left[\frac{1}{\tan(\theta_2)} + \frac{1}{\tan(\theta_1)}\right] \tag{2}$$

where D_f is core diameter of the optical fiber, Θ_1 and Θ_2 are determined by the numerical aperture of the fiber and the index of scattering medium.

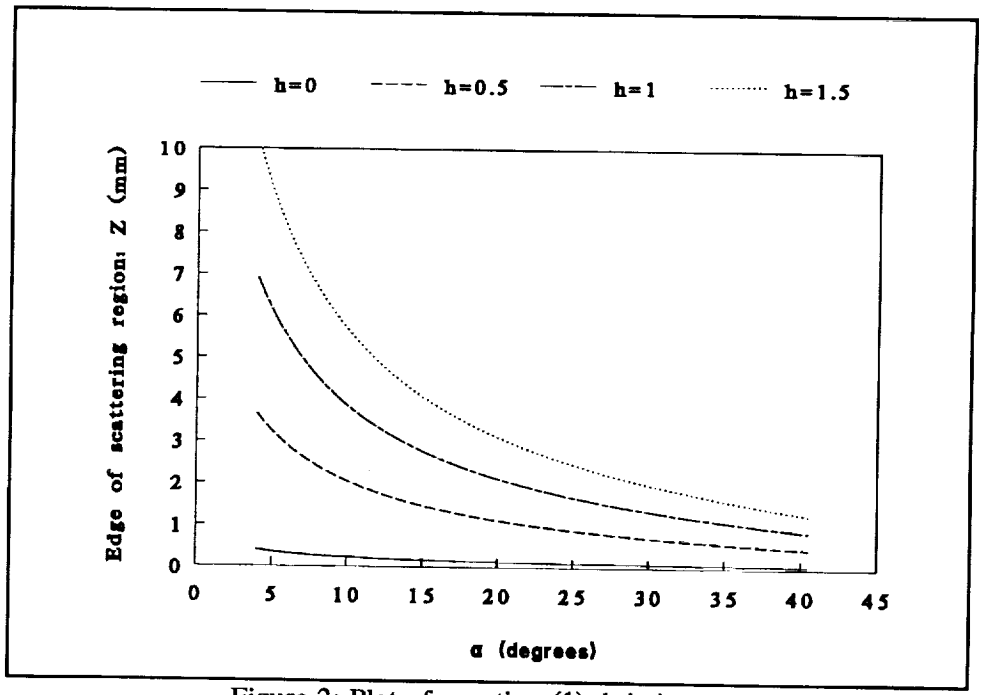

Figure 2: Plot of equation (1), h is in mm.

Figure 2 shows a plot Z as function of the inclination angle α and the separation h. Z should be as large as possible in order to allow interrogation of the scattering region within the interior of the scattering chamber. However, a large Z is accompanied by a reduction in the optical power density in the scattering region, due to the increase in the beam

diameter. The length ΔZ of the scattering region is also an important consideration, in order to maintain a small scattering volume. Figure 3 shows a plot of ΔZ as a function of α and h. A fiber probe based on the above criterion was designed for the QELS investigation of two protein systems, lysozyme and BSA. The fiber probe provides measurements at a backscatter angle of 143°. A monomode optical fiber is used for delivering a Gaussian beam, waist at the exit is equal to 2 μm, and a miltimode optical fiber is employed for the detection of the scattered light. Self-beating efficiency was sacrificed for increased count rate. As discussed by Dhadwal et al[3], in certain situation, choice of a multimode fiber as a receiver is more judicious.

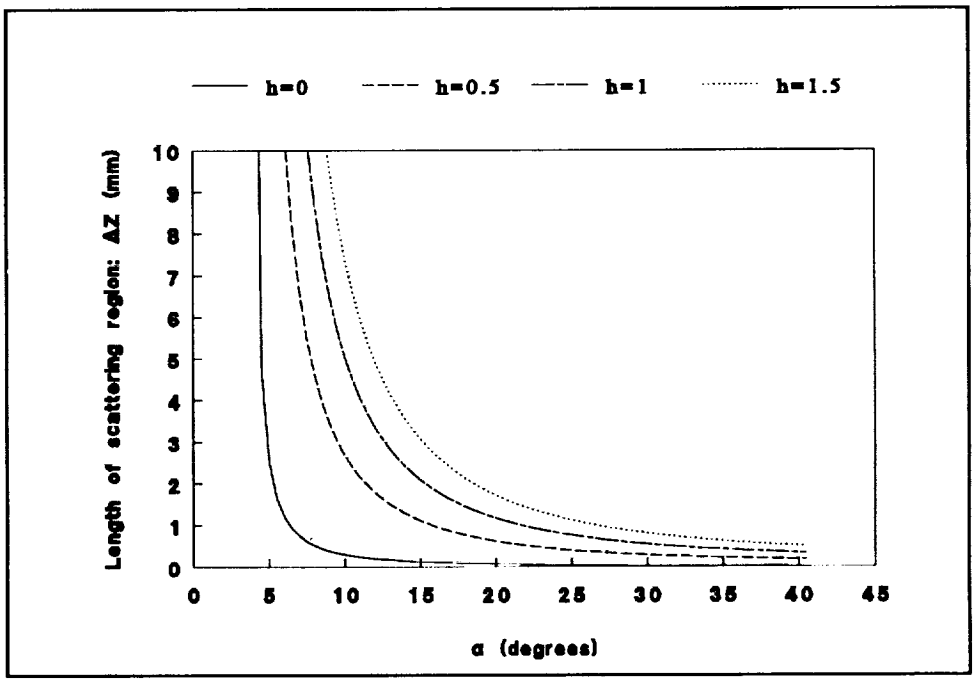

Figure 3: Plot of equation (2)

3. EXPERIMENTAL PROCEDURE

3.1 Sample preparation

Lysozyme (hen egg white, molecular weight 14,000) and bovine serum albumin, BSA (molecular weight 68,000) were obtained from Boehringer Mannheim Biochemicals. The lysozyme was purified by passing through Biosep-SEC-3000 size exclusion preparative column (600 mm x 21.2 mm) from Phenomenex with 50 mM sodium phosphate buffer at pH=6.8 as the mobile phase. The lysozyme monomer fraction was collected, exhaustively dialyzed against 40 mM sodium acetate buffer at pH=4.3 and concentrated to an appropriate level for light scattering measurements. The BSA was dissolved directly into a 50 mM sodium phosphate buffer at pH=7.0 and used without further purification.

Before making light scattering measurements, the protein solutions were cleansed by using a circulating filtration loop as shown in figure 4. A small amount of the protein solution (≈2 ml) was placed in a sample reservoir connected to a peristaltic pump using small diameter flexible tubing. The pump forced the solution through a 0.2 μ pore size filter from Gelman and then into the DLS cell. The loop was completed by returning the solution to the sample reservoir. Circulating the solution in this manner resulted in optically clean solutions and also allowed the protein concentration to be easily adjusted.

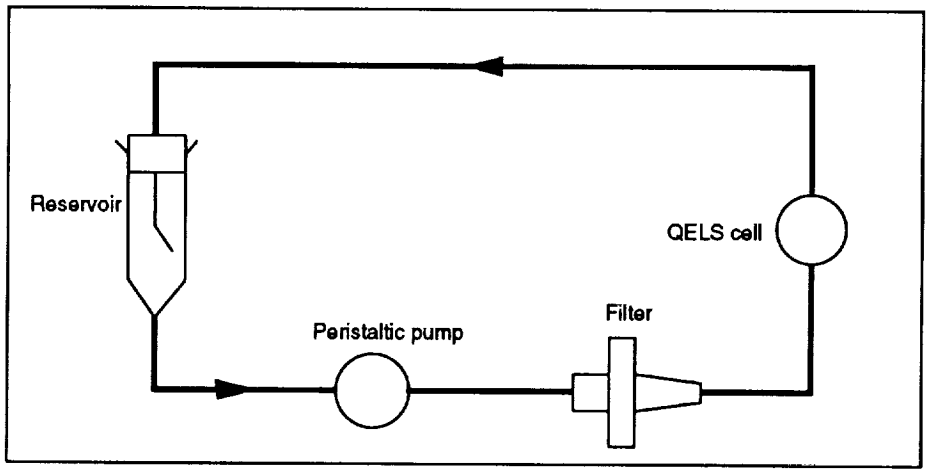

Figure 4: Schematic of the filtration process

3.2 Experimental set up

A backscatter fiber optic probe, as described in section 2, was positioned outside the sample cell as shown in figure 5. In this preliminary study, light from a helium-neon laser (Spectra Physics model 124B) was launched into the transmitting monomode optical fiber by means of a microscope objective. The laser beam emanating from the tip of the probe body had a waist diameter of 4 μm and a power of 2 mW at wavelength of 632.8 nm. The receiving multimode fiber provided collection of the scattered light at an angle of 143°. The free end of the receiving fiber was connected to a photomultiplier tube.

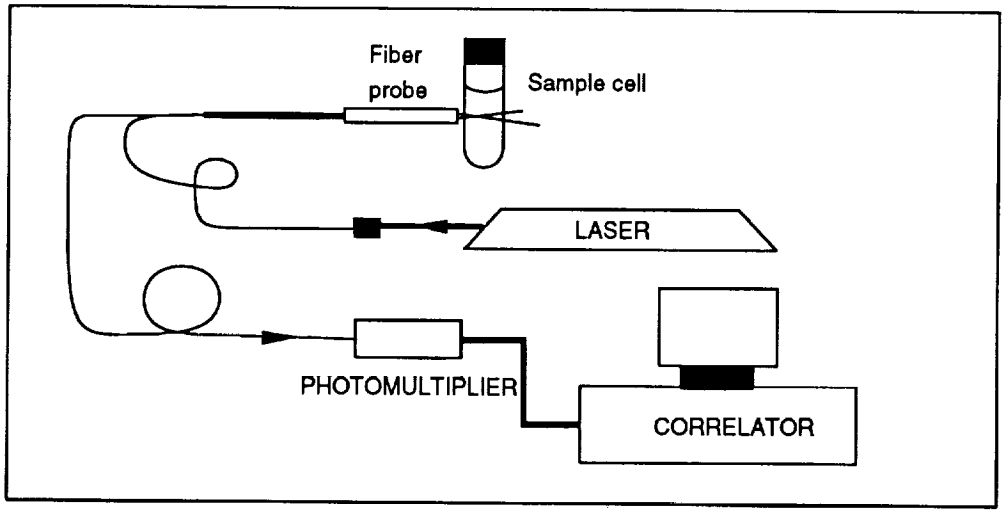

Figure 5: Schematic of the experimental set up

A conventional laser light scattering spectrometer (Brookhaven Instruments model BI-200SM) provided the capability for making QELS measurements on the exact same sample. The system operated at a wavelength of 514.5 nm with a optical power level of 40 mW. The laser was focussed into the scattering cell, which was placed in an index matching, thermostatically controlled vat. The scattered signal could be collected over a range of scattering angles using the detector optics mounted on a goniometer.

4. RESULTS AND DISCUSSION

The scattered photon stream, after amplification, discrimination and shaping, was correlated using a digital correlator (Brookhaven Instruments model BI2030). Figure 6 shows a comparison of the normalized intensity autocorrelation obtained from a 12.47 mg/ml sample of BSA. Triangles and squares denote measurements made with the conventional and fiber optic systems, respectively. As is expected the measurements with fiber probe are relatively more noisy. The noise in autocorrelation could be decreased further by increasing the accumulation time. Autocorrelation functions were recorded at three different concentrations of BSA and lysozyme. Data inversion techniques for recovering a characteristic size distribution from the autocorrelation data have been described elsewhere in greater detail[15]. Here it suffices to say that the recovery of the particle size distribution involves inversion of a Laplace transform; an ill-posed inversion problem. In our analysis we used the non-negative least squares technique for recovering the size distribution[16]. The necessary software was provided by the manufacturers of the correlator. Figure 7 shows the particle size distributions recovered from the data in figure 6. Table I summarizes the characteristic size of the protein monomers under various dilutions. The data obtained with the fiber probe shows good agreement with the conventional measurements made under more favorable experimental conditions. Both techniques give close agreement with the values found in the literature[17].

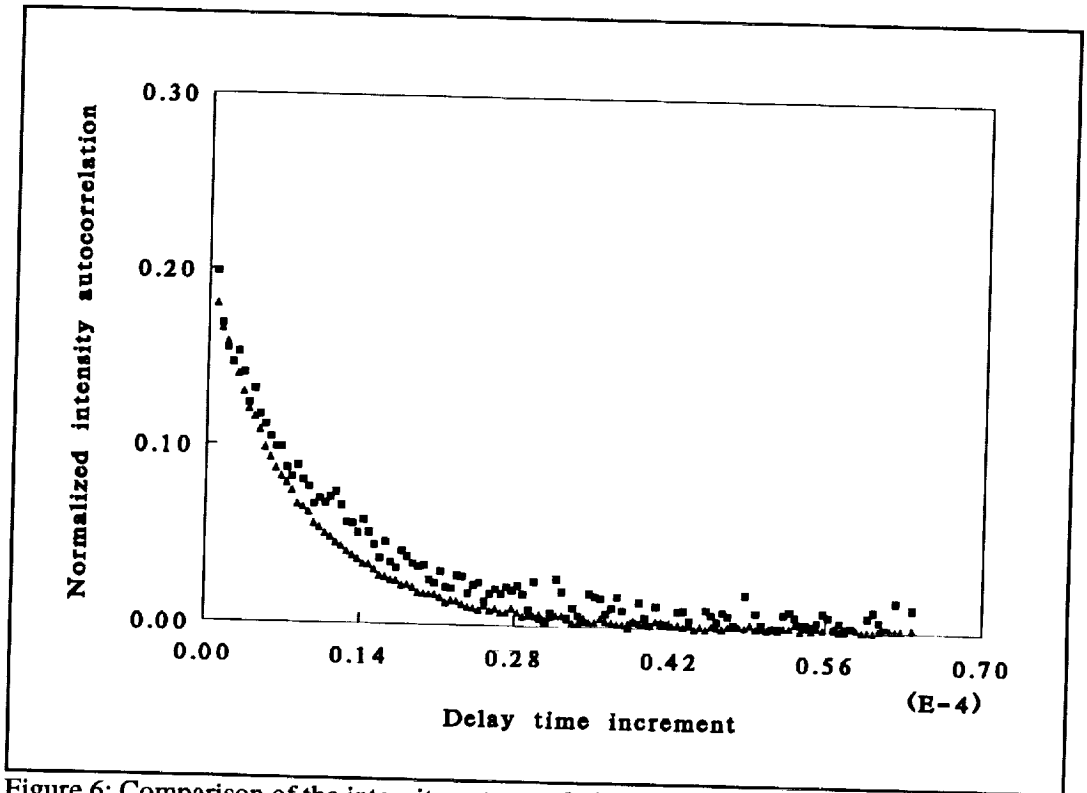

Figure 6: Comparison of the intensity autocorrelation data obtained from BSA at C=12.47 mg/ml. triangles - conventional system and squares - fiber optic probe.

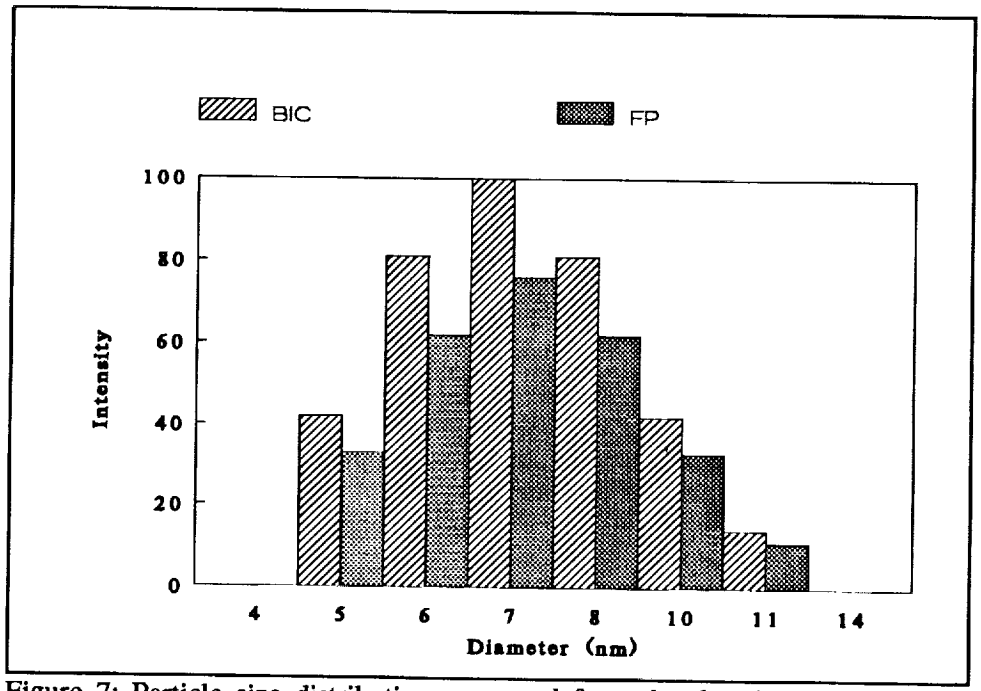

Figure 7: Particle size distribution recovered from the data in figure 6. BIC- conventional QELS system, FP - fiber probe

Table I: Summary of results. BIC - conventional QELS system.

PROTEIN SAMPLE	CONCENTRATION (mg/ml)	AVERAGE SIZE (nm)	
		BIC	Fiber Probe
Lysozyme	7.32	3.36	3.25
	12.42	3.05	2.94
	24.40	3.49	3.00
Bovine serum albumin	12.70	7.00	8.42
	8.85	6.82	6.35
	5.50	7.47	7.42

5. SUMMARY

The preliminary measurements reported here have demonstrated the utility of backscatter fiber optic probes for use in QELS studies of weak scatterers in the dilute regime. The fiber probe can be integrated to a semiconductor laser and to a miniature photomulitplier or an avalanche photodiode. Additionally, we expect considerable improvements in the signal-to-ratio by integrating gradient index fiber lenses to the monomode fibers as described by Dhadwal et al[7].

6. ACKNOWLEDGEMENTS

The authors would like to thank NASA's microgravity Sciences and Applications Division, code SN, and HSD wishes to acknowledge support from the same division under contract number NCC3-241.

7. REFERENCES

1. Harbans S. Dhadwal, Rafat R. Ansari and Michael A. DellaVecchia, "A Coherent Fiber Optic Sensor For Early Detection of Cataractogenesis in a Human Eye Lens", Optical Engineering:special issue on Biomedical Engineering, Feb (1993)

2. Harbans S. Dhadwal, Rafat R. Ansari and William V. Meyer, "A fiber optic probe for particle sizing in concentrated systems," Review of Scientific Instruments, 63, 2963-2968 (1991)

3. H.S.Dhadwal, C.Wu and B. Chu,"Fiber Optic Detector Probes For Laser Light Scattering", Applied Optics,28, 4199-4205 (1989)

4. H.S.Dhadwal and B.Chu,"A Fiber Optic Laser Light Scattering Spectrometer", Review of Scientific Instruments, vol. 60, pp.845-853 [also published in SPIE Milestone Series. Vol. MS 12, "Selected Papers on Laser Light Scattering by Macromolecular, Supramolecular and Fluid Systems,"edited by B.Chu (1990)

5. H.S.Dhadwal and B.Chu,"Fiber Optics in Laser Light Scattering Spectroscopy",J. Colloid and Interface Science, vol. 115, pp.561-563 (1987)

6. Rafat R. Ansari, Harbans S. Dhadwal, H.M.Cheung, and William V. Meyer, "Microemulsion characterization using a fiber optic probe", Photon Correlation and Scattering: Theory and Applications, Eighth Topical Meeting, Boulder, Colorado, August 24-26, 1992

7. Harbans S. Dhadwal, Romel Khan and Kwang Suh, "An integrated fiber optic probe for photon correlation spectroscopy", Photon Correlation and Scattering: Theory and Applications, Eighth Topical Meeting, Boulder, Colorado, August 24-26, 1992

8. Rafat R. Ansari, Harbans S. Dhadwal, Michael A. Dellavecchia and Melanie Campbell ,"A fiber optic sensor for ophthalmic refractive diagnosis," Proceeding of the International Society of Optical Engineering: Fiber Optic Medical and Fluorescent Sensors and Applications, Los Angeles, 19-24 January 1992, vol. 1648, pp.83-105

9. Harbans S. Dhadwal and Rafat R. Ansari,"A multiple fiber optic probe for several applications," Proceeding of the International Society of Optical Engineering: Fiber Optic and Laser Sensors IX, vol. 1584, pp 262-272; Boston, MA; 3-6 September 1991

10. Harbans S. Dhadwal "A Back Scatter Fiber Optic Probe For Particle Sizing," Gradient-Index Optical Systems, 1991, Technical Digest Series (Optical Society of America, Washington, DC, 1991), pp.165-167

11. R.G.W. Brown, "Dynamic light scattering using monomode optical fibers," App. Opt., vol. 26, 4846-4849 (1987)

12. D.A.Ross, H.S.Dhadwal and R.B.Dyott, "The determination of the mean and standard deviation of the sized distribution of a colloidal suspension of submicroscopic particles using the fibre optic Doppler anemometer, FODA," J. Colloid and Interface Sci., vol. 64, 533-542 (1978)

13. Auweter and D. Horn, "Fibre-optical quasi-elastic light scattering studies of concentrated dispersions," J. Colloid and Interface Sci., vol 105, 399-409 (1985)

14. N.C.Ford, "Theory and Practice of Correlation Spectroscopy," in *Measurement of Suspended Particles by Quasi-Elastic Light Scattering*, Baton E. Dahneke, John Wiley & Sons, Inc., New York (1983)

15. B. Chu, "Laser Light Scattering: Basic Principles and Practice," Academic Press, New York (1991)

16. C.L.Lawson and R.J. Hanson, "Solving Least Squares Problems," Prentice-Hall, New York (1974)

17. R. Foord, E. Jakeman, C.J. Oliver, E.R. Pike, R.J. Blagrove, E. Wood, and A.R. Peacocke, "Determination of diffusion coefficient of haemocyanin at low concentrations by intensity fluctuation spectroscopy of scattered laser light," Nature **227**, 242-245 (1970)